POLITECNICO DI MILANO

Corso di Laurea Specialistica in Ingegneria Biomedicaa

Dipartimento di Chimica, Materiali e Ingegneria Chimica "Giulio Natta"

Assessment of Dental Implant Stability by Means of the Electro-Mechanical Impedance Method

Relatori: Prof. Roberto CHIESA

Correlatore: Ing. Luigi DE NARDO

Correlatore: Prof. Piervincenzo RIZZO

Tesi di Laurea Specialistica di:

Giovanni BOEMIO

(Matricola 725505)

Anno Accademico 2009-2010

A mia madre.

Ringraziamenti

Un sincero ringraziamento va al Prof. Piervincenzo Rizzo che mi ha guidato e fatto sentire a mio agio durante la mia permanenza all'University of Pittsburgh, al Prof. Roberto Chiesa e Luigi De Nardo i quali mi hanno dato la possibilità di svolgere questo lavoro di tesi.

Desidero ringraziare mio padre Umberto, la sua compagna Rita e mio fratello Giuseppe per il supporto essenziale durante questo periodo della mia vita.

Infine desidero dire alla mia Mariane semplicemente una parola: obrigado.

Giovanni

Politecnico di Milano
Luglio 2010

Abstract

Introduction

Implant stability is a prerequisite for functional recovery in load-bearing prostheses. Robust, reliable, and non-invasive methods to assess the bone-interface of dental and orthopedic implants are increasingly demanded for clinical diagnosis and direct prognosis.

According to *Meredith* [84] implant stability is a two-step process that can be divided into primary and secondary phases and it is the result of the bone-healing time. Primary stability is achieved immediately after a surgical procedure and depends upon factors such as bone quality and quantity, surgical technique, and implant geometry. There is a wide consensus that the lack of primary stability represents the main risk factor for aseptic loosening of osseointegrated devices [80]. Secondary stability refers to the bone formation and remodeling processes, resulting in biological fixation through continuous bone apposition (contact osteogenesis) and remodeling [31, 61].

The development of effective approaches to functionally evaluate osseointegration has been actively promoted in recent years, both clinically or by means of instrumentations [72]. Several biomechanic, imaging, and nondestructive techniques have been developed for the evaluation of orthopedic [74], dental prostheses [76], or to assess the peri-implant wound healing and the prognosis of implant therapy [11]. One of the most common methods is the commercial system Periotest, introduced

by Schulte [118] to perform measurements of the damping characteristics of periodontal ligaments. Although the Periotest is broadly accepted, its reliability in measuring implant stability has been questioned.

Meredith [85] introduced a method based on Resonance Frequency (RF) analysis that employs a small L-shaped transducer screwed to the implant or abutment. The transducer is excited by a sinusoidal signal, typically comprised of between 5 kHz and 15 kHz. The dynamic response of the implant and particularly of the first resonance peak is measured as an indicator of the stability. The higher the resonance frequency, the more stable the implant.

In this study, the feasibility of the Electro-Mechanical Impedance (EMI) method to assess implant stability is discussed. In general, the approach uses one or more Piezoceramic Transducers (PZTs) attached to or embedded in the material (host structure) being probed. The transducer induces low-to high-frequency structural excitations when subjected to an electric field. The transducer's electrical admittance can be related to the mechanical impedance of the host structure, and therefore it can be exploited to assess the health of the host element.

The present study shows promising results and may pave the road toward an innovative approach for the noninvasive monitoring of implanted prostheses.

Materials and Methods

In this study, two series of tests were implemented:

ì Tests that simulate the inverse of the healing process;

ii Test that simulate the healing process

The first series involved the use of solid rigid polyurethane foams from Sawbones®, which are widely used to simulate the human bone. Foam specimens were dissolved by means of nitric acid and the decomposition process was monitored by measuring the EMI of the PZTs attached to the implants inserted in the foam.

The second series comprised four implants with attached PZTs inserted inside a solid joint compound specimen. To simulate the observation of formation of bone on the implant surface, the dental screws were entrenched in four alveoli filled with fresh compound. The fresh compound's setting was monitored over 9 days time.

Two types of implants, namely CORE with internal hexagon and PLUS with external hexagon from Bio Implant (Italy), were used. One implant type, hereafter indicated as the short implant, was 2.9 mm in diameter and 10 mm long. The second kind of implant, hereafter indicated as the long implant, was 5 mm in diameter and 15 mm long. The implants were entrenched in three different materials, namely Solid Rigid Polyurethane Foam (40 pcf), Cellular Rigid Polyurethane Foam (10 pcf), and a commercial joint compound. The foams were both from Sawbone® and they were respectively high-density polyurethane 640 Kg/m^3 (40 lb/ft^3) and low-density polyurethane 160 Kg/m^3 (10 lb/ft^3). The densities of the polyurethane foams were chosen because they are representative of two bone densities, according to the classification D1-D4 proposed by Misch [15]. The hard (denser) polyurethane can be related to a D1 bone, while the soft polyurethane can be considered representative of a D4 (softer) bone. Piezoceramics PSI-5A4E transducers from Piezo Systems, Inc. were used. They were custom cut to be circular (3.175 mm diameter and 0.1905 mm thickness) and square ($2\times2\times0.267$ mm^3), ($1\times1\times0.267$ mm^3) elements. The transducers' admittance was measured by means of an Agilent E4980A LCR meter connected to a multi-channel Agilent 34970A Data Acquisition Switch Unit. Both were controlled through a Visual Basic Application interface. Following up preliminary tests, the measurements were taken in the frequency range 0-1 MHz at 0.5 kHz interval. This interval is dictated by the best resolution achievable by the instrument.

Various authors have proposed different statistical indices to analyze and quantify the outcomes of EMI measurements [116, 41]. In this study the root mean square deviation (RMSD) and the root mean square (RMS) were computed and plotted as a function of time during both the inverse and direct healing simulated process.

The RMSD (%) is given by the following equation:

$$\left(\sum_{i=1}^{n}\sqrt{\frac{[G_j(\omega i)-G_0(\omega i)]^2}{[G_0(\omega i)]^2}}\right)\times 100$$

where $G_j(\omega i)$ is the conductance value of $\imath th$ frequency point of the $\jmath th$ decomposition time and $G_0(\omega i)$ is the baseline conductance value of the $\imath th$ frequency point, n is the upper limit of frequency range.

While the RMS:

$$\left(\sum_{i=1}^{n}\sqrt{\frac{G_j(\omega i)^2}{N}}\right)$$

where $G_j(\omega i)$ is the conductance value of $\imath th$ frequency point of the $\jmath th$ decomposition time and N represents the upper limit (i.e. in a range comprising of N frequencies). Finally uniaxial compression tests were performed according to UNI 6350-68 by using a uniaxial electromechanical system (Instron model 4200, load cell 1 kN) operated in displacement control. Five cylindrical specimens 12 mm in diameter and 12 mm high were punched out from a slice of 40 pcf high density polyurethane foam and immersed in a solution of nitric acid [w/w] = 68-70%. At each timepoint, specimens were removed from the acid bath and then were exsiccated at ambient temperature until they fully dried. The specimens were then tested at 1 mm/min crosshead rate, performing one loading/unloading cycle up to = 50% or up to the maximum deformation allowed by the load cell.

Figure 1 shows the polyurethane and the compound specimens.

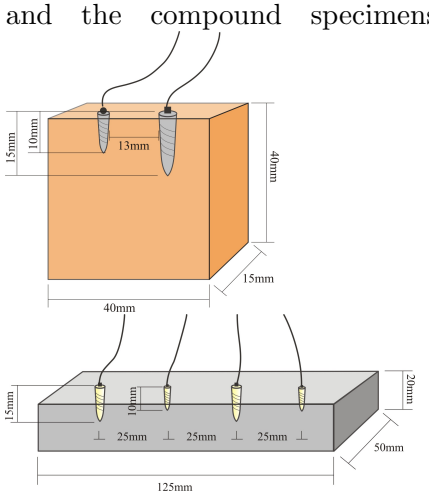

Figure 1. Polyurethane (top) and compound (bottom) specimens

Results

The results associated with the tests that simulate the inverse of healing process showed an increase of the conductance (real part of the admittance), as the decomposition by means of nitric acid progresses, whereas a decrease of the resonance peak due to the damping of the structure is observed. The figure 2 shows the conductance associated with the hard polyurethane for the short (top) and the long (bottom) implant.

The RMSD of the conductance as a function of the monitoring time for both implants is presented in figure 3. For the first six hours, the RMSD shows the same trend for both implants. Then the RMSD associated with the square PZT presented a plateau. A five percent divergence is visible around 10 h. In the figure 3 the dots and the x represent the short and the long implant respectively.

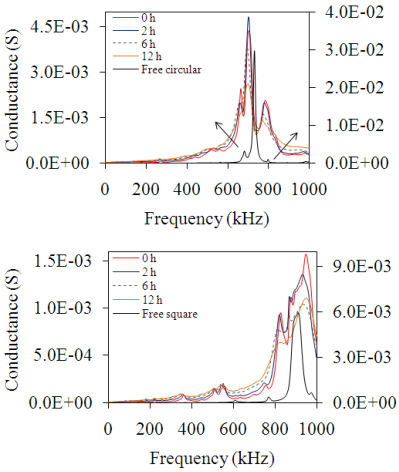

Figure 2. Conductance as a function of frequency for short (top) and long (bottom) implant

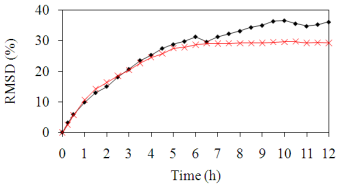

Figure 3. RMSD as a function of time for short (dots) and long (x) implant

The results of the mechanical test in terms of stress vs strain is presented in figure 4. The graphs associated to the mechanical responses of the coupons exposed to the action of the acid for 2 and 12 hours are presented and are overlapped to the response from the baseline specimen.

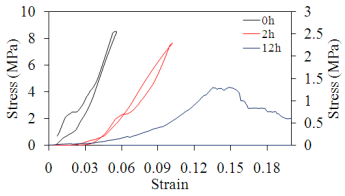

Figure 4. Stress-strain plot for different degradation time

From the plot in figure 4 the Young modulus of the material was computed. The value of the percentage Young modulus loss as a function of the degradation time is presented in figure 5. Such value is plotted against the right ordinate axis. To compare the results of the mechanical test with the results from the decomposition test, the values of the RMDS associated with both short and long implants are overlapped.

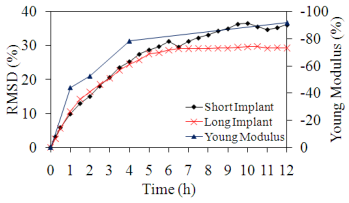

Figure 5. Young modulus loss as a function of time, overlapped to the RMSD signature

The qualitative agreement between the mechanical test and the EMI measurements is evident.

In the second test, the capability of the EMI method to assess the soundness of implants in soft bones was evaluated. As said earlier, the density of the polyurethane specimen used in this test is considered to be related to D4 soft bone, which has an elastic modulus of 35 MPa. The responses observed in these figures are similar to the hard polyurethane, namely an increase in the conductance at frequencies outside the peak resonance ranges, and a decrease of the peaks' amplitudes due to the increase of damping.

In conclusion, for as regards the joint compound test, in figure 6 the conductance associated to the long and short implant is presented.

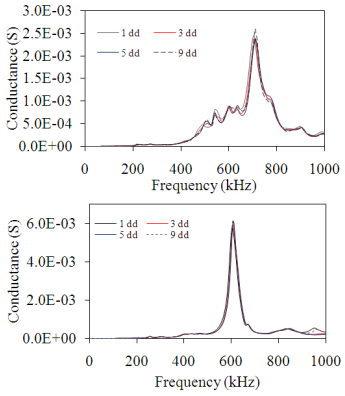

Figure 6. Conductance as a function of frequency for long (top) and short(bottom) implant

A gradual shift towards to the higher frequencies is observed. On

the contrary, the values of the conductance outside the peak cones increase with the monitoring time.

Discussion

Different implant geometries, bone like materials and trasducers were used in order to prove the effectiveness and reliability of the electromechanical impedance method for the assessment of implant stability. The dynamical interaction over the time among the structure and the PZT was monitored. Therefore, features as mass, stiffness and damping have to be taken in account in order to assess the frequency response of the structure. Regarding the decomposition process the conductance underwent to progressive increase by increasing degradation time. It can be argued that the values of the conductance within these ranges are related to the polyurethane stiffness. As proved by *Brosh et al* [111], the stiffness of the bone-implant interface during healing time increases due to anchorage of the bone to the implant surface. Therefore it can be inferred that the EMI method will be indirectly able to assess the stiffness of the bone-implant system by monitoring the admittance characteristics of a PZT attached to the implant. Moreover, it is believed that the shift to the lower frequencies is associated with the decrease of the polyurethane stiffness as shown in figure 7.

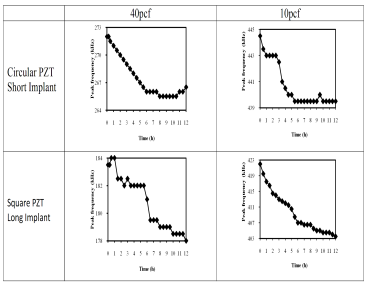

Figure 7. Comparison of peak frequency for decomposition test

In addition, such shift to lower frequencies is evident both for different implant geometries and polyurethane stiffness, therefore, it can be concluded that the EMI response is robust enough to different boundary conditions.

Considering the healing test the results confirm what it has been said for the denser foam and demonstrate the effectiveness of the EMI to monitor the evolution of the material stiffness as well

as the stiffness of the material-implant interface. In addition, the results agree with the findings of *Soh and Bhalla* [22] and *Shin et al* [110] where the curing age of concrete was monitored by means of EMI. They found similar results in terms of stiffness, in fact, a shift to higher frequency is observed as the curing time increases; nevertheless with the respect to the damping the results were somehow discordant.

Conclusion

In this paper a feasibility study about the use of the electromechanical impedance method to assess the stability of dental implants is presented. Experiments showed a shift of the frequency peaks toward the lower frequencies when degradation was observed and toward higher frequencies when setting was monitored.

The quantitative values of the RMSD were then compared to the stiffness and the Young modulus of high-density polyurethane exposed to the same solution of nitric acid. These material properties were obtained through uniaxial-tensile loads. The correlation between the electro-mechanical results and the destructive test was demonstrated.

Although SAWBONE is universally recognized as a material that reproduces bone tissue well, joint compound does not. Therefore, it must be acknowledged that the amount of fresh compound around the screw might not have been thoroughly representative of the amount and quality of bone tissue that forms around real implants during the healing process.

It is believed that this study provided sufficient experimental evidence to encourage further study on the application of EMI for dental implant assessment.

Sommario

Introduzione

La stabilità degli impianti dentali è un prerequisito per il recupero funzionale di protesi dentarie. Metodi robusti, affidabili e non invasivi per valutare l'osteointegrazione degli impianti dentali ed ortopedici sono sempre più richiesti per una corretta diagnosi e la prognosi clinica.

La stabilità degli impianti dentali è un processo che può essere diviso in primaria e secondaria e che costituisce il risultato nel tempo del complesso di fenomeni che caratterizzano l'osteointegrazione [84]. La stabilità primaria è raggiunta subito dopo la procedura chirurgica e dipende da fattori quali qualità e quantità dell'osso, tecnica chirurgica e geometria dell'impianto. C'è un ampio consenso che la mancanza di stabilità primaria rappresenta il fattore di rischio principale per il fallimento dei dispositivi osteointegrati [80]. La stabilità secondaria si riferisce alla formazione dell'osso ed al processo di rimodellamento, con conseguente fissazione biologica attraverso l'apposizione continua dell'osso (osteogenesi di contatto) e rimodellamento [31, 61].

Lo sviluppo di metodi efficaci per valutare dal punto di vista funzionale l'osteointegrazione sono stati abbondandemente esaminati negli ultimi anni, sia clinicamente che sperimentalmente. Diverse tecniche non distruttive sono state sviluppate per la valutazione delle protesi ortopediche [74] e dentali in termini di guarigione peri-implantare e valutazioni prognostiche [76, 11]. Uno dei metodi più comuni è il Periotest, introdotto

da Schulte [118] per misurare le caratteristiche elastiche dei legamenti periodontali. Sebbene il Periotest sia accettato largamente, la sua affidabilità nel valutare la stabilità degli impianti dentali è messa in discussione.

Meredith [85] ha introdotto un metodo basato sulle frequenze di risonanza (RF) che impiega un piccolo trasduttore a forma di L avvitato all'impianto o all'abutment. Il trasduttore è eccitato da un segnale sinusoidale, tipicamente fra da 5 kHz e 15 kHz. La risposta dinamica dell'impianto, e in particolare, la misura del primo picco di risonanza fornisce un'indicazione della stabilità. Più è alta la frequenza di risonanza, più stabile è l'impianto.

In questo lavoro di tesi, è discussa la possibilità di valutare la stabilità degli impianti dentali attraverso il metodo dell'impedenza elettromeccanica (EMI). Il metodo utilizza generalmente uno o più trasduttori piezoceramici incollati o integrati nel struttura ospite. Il trasduttore, sottoposto ad un campo elettrico, induce vibrazioni nella struttura. La misura elettrica dell'ammettenza del trasduttore può essere correlata con l'impedenza meccanica della struttura e quindi può essere sfruttata per valutare la presenza di difetti nella stessa.

Materiali e Metodi

In questo studio sono stati effettuati, due serie di test simulanti l'inverso del processo di guarigione ossea che il processo diretto di guarigione osseo.

La prima serie ha compreso l'uso di schiume in poliuretano rigido (Sawbones®), ampiamente utilizzato per simulare l'osso trabecolare. I campioni in poliuretano sono stati attaccati chimicamente per mezzo di acido nitrico ed il processo di decomposizione è stato controllato misurando l'ammettenza del PZT incollato sugli impianti inseriti nella schiuma.

La seconda serie ha compreso quattro impianti inseriti in un campione di gesso osservando l'indurimento del materiale nell'alveolo che conteneva ogni impianto sui quali erano incollati i

PZTs. Per simulare l'osservazione di formazione di osso sulla superficie dell'innesto, le viti dentarie sono state inserite in quattro alveoli riempiti di gesso fresco. L'indurimento del composto fresco è stato controllato per diversi giorni.

Due tipi di impianti sono stati utilizzati, CORE con esagono interno e bio-PLUS con esagono esterno, cortesemente forniti da IMPLANT (Italia). Un tipo di impianto, di seguito indicato come impianto corto, era di 2,9 mm di diametro e di 10mm di lunghezza. Il secondo impianto, di seguito indicato come impianto lungo, era di 5 millimetri di diametro e di 15 millimetri di lunghezza. Gli impianti sono stati inseriti in tre materiali differenti, cioè una schiuma poliuretanica solida rigida (pcf 40), una schiuma poliuretanica cellulare rigida (pcf 10) e un composto di gesso. Le schiume (Sawbone®) erano rispettivamente poliuretano ad alta densità 640 Kg/m^3 (40 lb/ft^3) e poliuretano a bassa densità 160 Kg/m^3 (10 lb/ft^3). Le densità delle schiume di poliuretano sono state scelte perché rappresentano due densità dell'osso, secondo la classificazione D1-D4 proposta da Misch [15]. Il poliuretano (più denso) duro può essere collegato con un osso D1, mentre il poliuretano soft può essere considerato rappresentante di un osso (più soft) D4. Sono stati utilizzati trasduttori piezoceramici PSI-5A4E (Piezo Systems, Inc.) quadrati di dimensioni ($2\times2\times0.267$ mm) e ($1\times1\times0.267$ mm) e circolari di dimensioni (diametro da 3.175 mm e 0.1905 mm di spessore). L'ammettenza è stata misurata per mezzo dello strumento della Agilent E4980A LCR collegato ad un multiplexer Agilent 34970A. Entrambi gli strumenti erano controllati attraverso interfaccia Visual Basic. I test sono stati eseguiti tra 0-1 MHz con un intervallo 0.5 kHz. Questo intervallo è dettato dalla migliore risoluzione realizzabile dallo strumento.

Vari autori hanno proposto indici statistici differenti per analizzare e quantificare i risultati delle misure di ammettenza [116, 41]. In questo studio la radice quadratica

media (RMS) e la radice quadratica media deviata (RMSD) sono state ricavate e plottate in funzione del tempo per entrambi i test eseguiti.

La RMSD(%) è data dalla seguente equazione:

$$\left(\sum_{i=1}^{n}\sqrt{\frac{[G_j(\omega i)-G_0(\omega i)]^2}{[G_0(\omega i)]^2}}\right)\times 100$$

dove $G_j(\omega i)$ è la conduttanza all'$\imath th$ frequenza del $\jmath th$ tempo di decomposizione e $G_0(\omega i)$ è la conduttanza di riferimento (baseline) all'$\imath th$ frequenza, n è il valore massimo di frequenza.

La RMS è data dalla seguente equazione:

$$\left(\sum_{i=1}^{n}\sqrt{\frac{G_j(\omega i)^2}{N}}\right)$$

dove $G_j(\omega i)$ è la conduttanza all'$\imath th$ frequenza del $\jmath th$ tempo di decomposizione e N rappresenta il valore massimo di frequenze misurate.

Infine, sono state eseguite prove di compressione monoassiali secondo le norme UNI 6350-68 attraverso un sistema elettromeccanico monoassiale (modello 4200 di Instron, 1 kN carico massimo). I provini cilindrici (12 mm di diametro e 12 mm di altezza) sono stati estratti da una lastra di schiuma poliuretanica ad alta densità 40 pcf e sono stati immersi in una soluzione di acido nitrico [w/w] = 68-70%. Dopo pre-determinati intervalli di tempo sono stati rimossi dal bagno acido ed essiccati a temperatura ambiente fino a completo asciugamento.

La Figura 1 mostra uno schema dei campioni di poliuretano e gesso utilizzati.

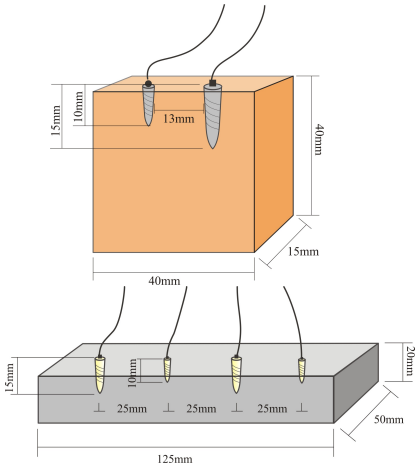

Figura 1. Campione in poliuretano (in alto) e in gesso (in basso)

Risultati

I risultati associati alle prove che simulano l'inverso del processo di guarigione hanno mostrato un aumento della conduttanza (parte reale dell'ammettenza), con il procedere della decomposizione per

mezzo dell'acido nitrico, mentre una diminuzione dei picchi di risonanza dovuti allo smorzamento viscoso prodotto dallo stesso. Figura 2 mostra la conduttanza per l'impianto corto (in alto) e lungo (in basso).

La RMSD della conduttanza in funzione del tempo di monitoraggio per entrambi gli impianti è presentato nella figura 3. Per le prime sei ore, la RMSD mostra la stessa tendenza per entrambi gli impianti. Dopodichè, la RMSD associata all' impianto corto presenta un plateau. Una divergenza del 5% è visibile a circa 10h. Nella figura 3 i punti e le x rappresentano rispettivamente l'impianto corto e lungo.

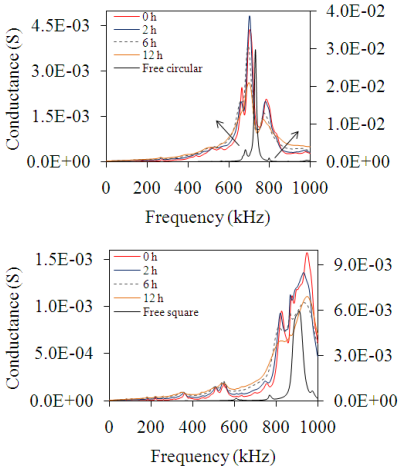

Figura 2. Conduttanza in funzione della frequenza per l'impianto corto (in alto) e lungo (in basso)

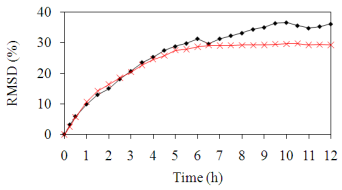

Figure 3. RMSD in funzione del tempo per l'impianto corto (punti) e lungo (x)

I risultati delle prove meccaniche in termini di sforzo/deformazione sono presentati nella figura 4. Il grafico rappresenta la risposta meccanica dei campioni esposti all'azione dell'acido per 2 e 12 ore e la risposta del campione non sottoposto a nessuna degradazione, indicato come 0h.

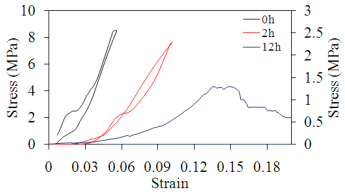

Figura 4. Sforzo-deformazione per differenti tempi di degradazione

Dalla figura 4 è stato ricavato il modulo di Young. Il valore di perdita percentuale del modulo in funzione del tempo di degradazione è presentato nella figura 5. Tale valore è visibile nell'asse delle ordinate a destra. Per confrontare i risultati delle prova meccaniche

ai risultati dalle prove elettromeccaniche, sono sovrapposti i valori della RMDS associati ad entrambi gli impianti.

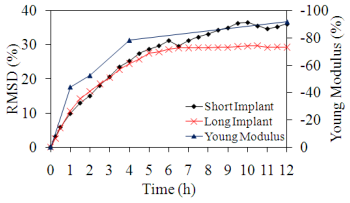

Figura 5. Modulo di Young in funzione del tempo, sovrapposto alla RMSD di entrambi gli impianti

Dalla figura si può notare come sia evidente la somiglianza dell'andamento del modulo di Young con la RMSD.

Nel secondo test è stata valutata la capacità del metodo EMI nel valutare la stabilità degli impianti nelle ossa meno dense. La densità del campione più soft è stata collegata con l'osso D4, che ha un modulo elastico del 35 MPa. Le risposte osservate sono simili al poliuretano duro, cioè un aumento nella conduttanza alle frequenze fuori dai picchi di risonanza e una diminuzione delle ampiezze dei picchi dovuto l'aumento di smorzamento.

In conclusione, per per quanto riguarda le prove effettuate con il gesso, la figura 6 mostra la conduttanza associata ad entrambi gli impianti (lungo in alto, corto in basso).

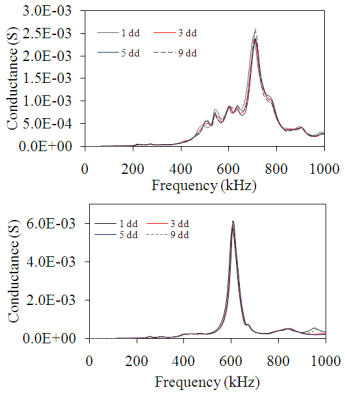

Figure 6. Conduttanza in funzione della frequenza per l'impianto lungo (in alto) e corto(in basso)

Si osserva uno shift graduale verso le alte frequenze. Contrariamente, i valori di conduttanza al di fuori dei picchi di risonanza crescono con il procedere del processo di indurimento.

Discussioni

Differenti geometrie, densità dei materiali e trasduttori piezoelettrici sono stati usati con lo scopo di dimostrare l'efficacia e l'affidabilità nella valutazione del metodo EMI. Ciò che è stato misurato è l'interazione dinamica nel tempo fra la struttura e il

PZT. Di conseguenza, caratteristiche come massa, rigidezza e smorzamento devono essere considerate per valutare la risposta in frequenza della struttura. Per quanto riguarda il processo di decomposizione la conduttanza ha subito un aumento progressivo con il procedere dell'attacco in acido nitrico. L'aumento della conduttanza è associata alla rigidezza del poliuretano. Come provato da *Brosh et al* [111], la rigidezza dell'interfaccia impianto-osso durante il processo di guarigione aumenta, come conseguenza dell'ancoraggio dell'osso sulla superficie dell'impianto. Di conseguenza, si può concludere che il metodo EMI può indirettamente valutare la rigidezza del sistema osso-impianto controllando le caratteristiche di ammettenza di un PZT interfacciato all'impianto. Inoltre, lo spostamento alle frequenze più basse è associato alla diminuzione della rigidezza del poliuretano come mostrato in figura 7.

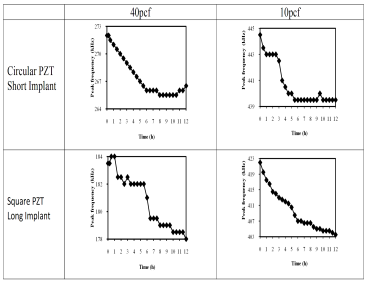

Figura 7. Confronto dei picchi in frequenza per differenti impianti e diversa densità del campione

Tale spostamento alle basse frequenze è evidente sia per la diversa geometria dell'impianto che per la differente densità del poliuretano, quindi, può essere concluso che la risposta di EMI è abbastanza robusta alle differenti condizioni al contorno.

Per quanto riguarda il test che simula il processo diretto di guarigione i risultati confermano quanto detto per la schiuma poliuretanica e quindi, dimostra l'efficacia dell'EMI nel controllare l'evoluzione della rigidezza del materiale e dell'interfaccia materiale-impianto.

Conclusioni

In questo lavoro di tesi è stato condotto uno studio riguardo l'uso del metodo dell'impedenza elettromec-

canica nel valutare la stabilità degli impianti dentali. In generale, può essere detto che gli esperimenti hanno mostrato uno spostamento dei picchi di frequenza verso le frequenze più basse durante il processo di degradazione, mentre verso le più alte frequenze durante il consolidamento del gesso.

I valori quantitativi della RMSD poi sono stati confrontati con il modulo elastico del poliuretano ad alta densità, esposto alla stessa soluzione di acido nitrico, ottenuto attraverso carichi monoassiali di compressione. E' stata dimostrata la correlazione con i risultati elettromeccanici.

Sebbene SAWBONE sia riconosciuto universalmente come materiale per riprodurre il tessuto osseo, il gesso non lo è altrettanto. Di conseguenza, si deve riconoscere che la quantità di gesso fresco intorno all'impianto non potrebbe essere completamente rappresentativo della quantità e della qualità di tessuto osseo che realmente si appongono durante il processo di guarigione.

In definitiva, si può concludere che questo studio ha fornito la prova sperimentale sufficiente per incoraggiare un proseguimento nelle sperimentazioni riguardo l'applicazione dell'EMI per la valutazione della stabilità, in funzione del tempo di guarigione, degli impianti dentali.

Contents

List of Figures

List of Tables

Chapter 1

Dental Implants

1.1 Classification of oral implants

A dental implant is an artificial device, placed in contact with oral connective and bone tissues, which has the function to replace the natural tooth root.

A dental implant is generally composed of three different parts (Figure1.1):

1. the fixture, which simulates the natural root;
2. the abutment, which connects the implant to crown. It is about 5 millimeters long and at its bottom there is a male external screw threading;
3. crown which replaces the natural tooth.

Generally, the implant is placed into the jawbone under the soft tissue; after 3-6 months of healing time (this period depending on several factors), in which a stable implant-bone interface is reached (osseointegration), the soft tissue is opened, thus the abutment is placed into the implant, then, the crown can be placed on the abutment (two stage procedure). However, over the years besides this procedure, another approach has been used, where both the implant and the abutment are

placed at the same time without the need of a secondary surgery (one stage procedure).

The type of implant used for each patient depends upon a complex interaction between functional and cosmetic needs, available bone, quality and quantity of remaining teeth, medical health, emotional temperament, treatment time and finances [*www.nycdentist.com*].

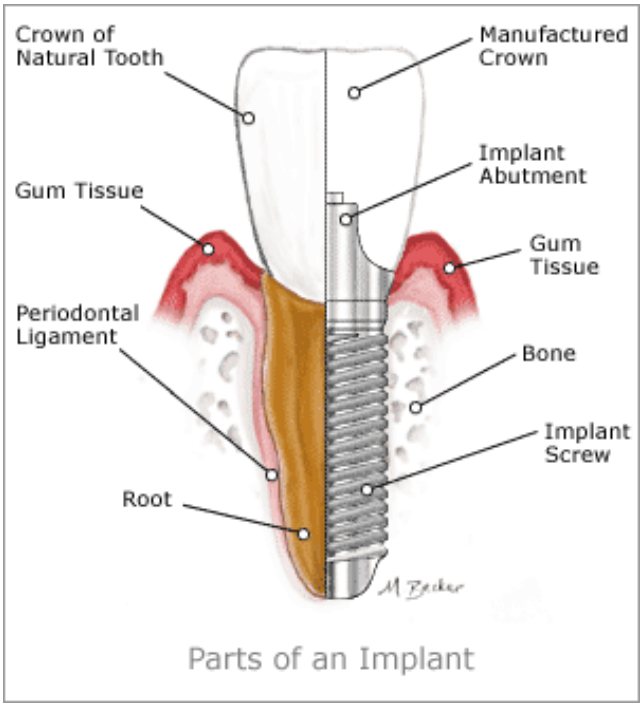

Figure 1.1: Parts of oral implant
(Source:www.deltadentalwi.com)

Today the most common implant used is the **endosseous implant**.

Historically it wasn't the first typology that the clinicians employed as the early attempts failed since both the surgical procedure and the materials were not evolved to provide their success.

Therefore, the first dental implants used are listed below:

- intramucosal [39] (no longer used);
- subperiosteal [38] (rapidly declining in use);
- transmandibular

- endosseous

Intramucosal implant involves cutting small intramucosal rententive areas in which to place buttons attached to the denture (Figure 1.2).

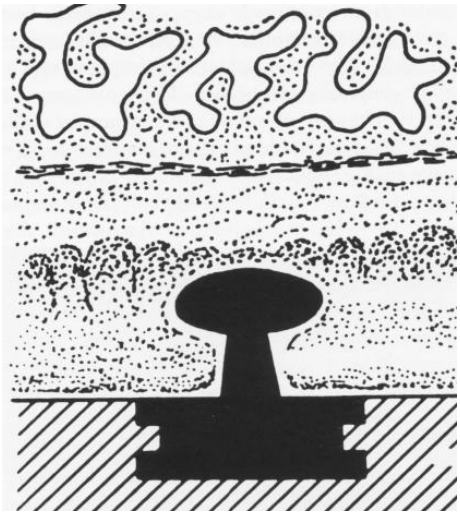

Figure 1.2: Intramucosal implant
([53])

The subperiosteal is an implant placed between the gingiva and the bone as show in the figure 1.4. The framework rests beneath the mucoperiosteum, with posts that penetrate the mucosa into the mouth, usually supporting an overdenture. This implant reported various porblems such as long term reliability, infection, and damage to the underlying bone.

Transmandibular implants, developed by *Bosker* in Netherlands, (figure 1.4) are similar to endosseous implants but they are designed to cross the entire jawbone until reach the bottom of the chin.

1.1.1 Endosseous implants

Nowadays, the endosseous implants gained popularity as they provide better outcomes than the previous ones. They are directly placed into the bone, hence, a bone-implant interface is formed; with the improvement of techniques and materials, which have lead to osseointegration, the endosseous implants completely replaced the previous ones. As a

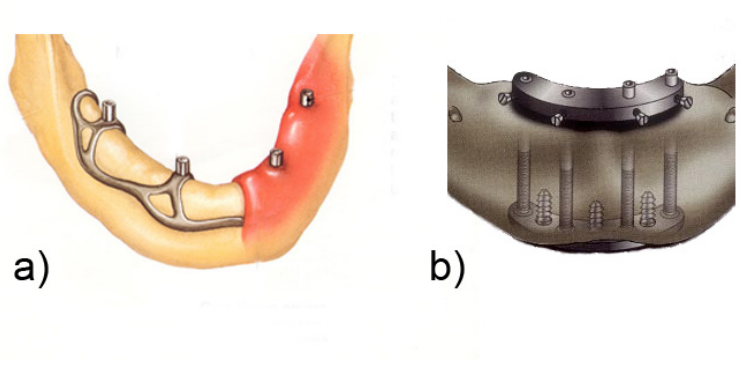

Figure 1.3: Subperiosteal (a) and transmandibular (b) implant
(Source:Quintessence Publishing Co.)

consequence, the market exploded considerably with more than 1300 implant designs combining various materials, shapes, size, diameters, lenghts, surfaces and connections [93].

The most utilized endosseous implants are the **root form implants**, which are similar to the natural tooth root. Typically, three types of root form implant are used based on design: cylinder, screw, combination of them [19]. The first, are usually pushed into the prepared bone site (press-fit), while the screw are threaded into the bone site. The cylinders are often coated with a rough material (e.g., hydroxyapatite, titanium plasma spray) to increase the surface area and therefore reduce the stress at the bone-implant interface; in fact, the screwed implant provide a surface area definitely greater than cylinder.

The screwed design is the most considered in literature and commercially (e.g., Branemark system, ITI system); it offers several advantages as greater surface area, surgical ease and not less important the removal ease if errors placement arise.

The upper implant's portion is called crest module; it has the function to allow the best connection with the abutment in order to achieve the stability of the two pieces; this is due to the flat to flat dimension of both the module and the abutment. The figure provides an appreciation about the frameworks.

Figure 1.4: Endosseous root form implant
(Source:www.nobelbiocare.com)

1.1.2 The materials

Dental implants can reach the clinical success if the following requirements are satisfied:

1. they must not be toxic to the cells in the surrounding tissues, or undergo dissolution and cause systemic damage to the patient;

2. they must be able to form a stable bone-implant interface that is capable of carrying occlusal loads, and transferring or distributing stresses to the adjacent bone so that bone vitality is maintained over long periods [75].

The majority of materials used for endosseous implants are metals and their alloys, especially the titanium but ceramics are also used. Metals and metal alloys present high corrosion resistance, strength, rigidity, ease of shaping and machining, and suitability for a wide range of sterilization techniques. Metals in general do not form an interfacial bond with bone. The process that leads to implant stability is typically an interlock in the bone and, moreover, using a variety of surface designs and textures bony

in-growth and the interfacial attachment is promoted [66]. Ceramics are generally hard materials with high compressive strengths; thanks to their crystalline structure, this materials are used because are bone-like and have similar physical properties to bone [124].

According to *Piliar* and *Hayashi* different chemical compositions of calcium phosphate ceramics based on specific ratios of calcium and phosphorus are used clinically for titanium implants (hydroxyapatite coatings) because is believed to contribute to more rapid osseointegration and greater amount of bone-implant contact than uncoated titanium in the early stages of healing [98],[71].

Zablotsky demonstrates that in the long term (after 12 months of placement) there is no difference between Ha coatings and uncoated implants [82].In fact, bone contact with titanium may be more favourable in the long-term [109].

Moreover, other studies pointed out that the main problem with hydroxyapatite coating is due to its dissolution and weakening that leads to its dissociation from the central titanium implant [79].

Two forms of titanium (Ti) are principally used for endosseous dental implants:

1. commercial pure titanium (c.p Ti): at least 99,5% pure Ti;
2. titanium alloy (Ti-6Al-4V).

A stronger bone implant interface may be achieved with cpTi than with Ti-6AI-4V, as greater removal torque forces were needed to loose the interfacial connection between cpTi implants and the surrounding bone [12]. The Ti alloys, in fact, prevent bone formation probably because of the release of aluminium ions wich can slow down bone cell differentiation [54, 103, 43].

Finally is possible to conclude that titanium is the main material in implant dentistry as its excellent corrosion resistance since the surface oxidises spontaneously upon contact with air or tissue fluids [36].

1.2 Osseointegration:general concecpts

In order to understand the process of osseointegration it is believed are useful two fundamental aspects, that are involved; the physical contact between the material's surface and extern enviroment, and the reaction of the bone to different loads.

1.2.1 Biomaterials and interface

A foreign material placed into the tissue produces a twofold effect: firstly, the surgical procedure produces a tissue damage; secondly, the new material will interact with it. From this point of view, some questions arise, for istance, if the material surface affects the healing process and in which way. In fact, when a biomaterial is inserted into the tissue the only part which reacts is the surface, therefore is important to consider the surface properties in order to figure out what might be the interaction process. The surface consist of the outermost atomic layer of the solid and its chemical composition can differ from that of the corresponding bulk. Placing a fresh surface in a foreign environment, a close contact between the environment occurs. The enviroment may be a gas, a liquid, or a complex biological system. The potential of interaction between the surface and the environment underlines the process in act.

Once identified this aspect, it is interesting to figure out what molecular processes occur at implant-tissue interface:

- *ion release and surface remodeling*: most biomaterials are not inert but undergoes some corrosion or degradation;
- *water-surface interaction*: contact with the physiological fluid leads to water adsorption at the implant surface, but, obviously, this depends on the type of the surface [88]. Various ionic species are also present at the surface and they may bond with it. The surface layer of the implant is therefore initially covered by an hydration layer consisting of water molecules, hydroxyl groups and ions;

- *biomolecules adsorption*: later arrive of water molecules and ions it's visible the adsorption on the surface with proteins that is due to several surface properties such as hydrophilic and hydrophobic rate, surface charge and polarity [26];
- *relation to cellular activity*: later the formation of the adsorbed layer of water, ions and biomolecules will interact with cells.

From this point of view, based upon the properties of the original surface as well as the type and state of the host tissue, this complex interface interaction may or may not lead to the successful co-existence of the tissue and the implant.

1.2.2 Understanding bone loading

The main features of the bone are to assure structural support and calcium metabolism [122]. The strength of the bone is directly related to the loading. When the bone is not adequately loaded it undegoes to reabsorption, moreover, the skeletal system attempts continuosly to adapt itself in order to achieve optimal strength with minimal mass. Indeed, bone cells are sensitive to the strain due to dynamic loading. Frost [51] proposed a descriptive theory of bone response to mechanical stress. According to this theory, there is a physiological strain range where bone is in equilibrium, determined by metabolic factors alone. The lower limit of this range is given by a "remodeling" process (*coupled process of bone resorption-formation*) while the upper limit of this range is given by a "modeling" one (*process of new bone deposition without prior resorption, or bone resorption not necessary followed by deposition*).

1.2.3 Definition of osseointegration

Osseointegration is commonly defined as a direct and stable anchorage of the implant by the formation of bone tissue without growth of fibrous tissue at the bone-implant interface. The term "osseointegration" was

for the first time introduced by *Branemark et al* in 1969 [89] in which they provided several factors that can lead to long term stability of dental implants. Since surgical intervention is carried out to place the implant, some aspects are to be considered in order to understand the good integration of the implant with the bone:

- *osteoconduction*: is the most important factor of early peri-implant healing, it means the recruitment of osteogenic cells and their migration to the implant surface;
- *formation of the new bone*: osteoblast cells produce secrete matrix that becomes mineralized as bone tissue;
- *bone remodeling*: which represents the turnover of the bone [65].

However, it is difficult to assess osseointegration as a "standard process" as each case differs from the other because of many reasons. The main are resumed in succession:

1. **bone quality**: the most popular method to assess bone quality is related to Lekholm and Zarb; they introduced a scale from 1 to 4, which Class 1 bone is predominantly cortical as in the interior mandible, while Class 4 bone is almost all trabecular as found in the posterior maxilla [114]. Indeed, clinical reports suggest that dental implants for the mandible have higher survival rates than those for the maxilla [29, 112];
2. **gaps between implant and bone**: healing process proceeds as described above, in which the gap is filled by blood clot soon after surgery. Then, if the implant is stable in the site, new bone growth on the surface [50];
3. **pre-existing bone that is damaged by surgical procedure**: the surgery damages pre-existing bone around an implant. *Hoshaw et al*[108] demonstrated a correlation between microdamage at the

interface and bone remodeling cycle; their works suggest that microdamage in bone stimulates bone remodeling;

4. **loading conditions**:this factor meets discordant opinions, whether loading the implant during healing period does not disturb the process of new bone formation. In fact, *Branemark et al*, in 1977,[90] defined a no-healing period of at least 3 months for the mandible and 6 months for the maxilla. *Ducheyne et al* confirmed, in 1977,[87] that bone ingrowth was not achieved into porous implants because of movement at the interface under dynamic loading. According to others similar experimental studies, it can be concluded that micromovements do not lead to osseintegration and should be avoided. In contrast, others studies stated that implants under loading, during healing period, achieve osseointegration anyway, for istance, *Deporter et el*,[2] performed implant loading after only 4 weeks of healing. Finally other authors retain the possibility of tolerated micromotion which does not lead to fibrous tissue ingrowth. From this point of view, *Cameron et al* introduced the concept of threshold micromovement [48]. *Piliar* [99] believed that a micromotion of 30 μm did not interfere with bone repair;

5. **implant design**: studies reported the use of different implants design, for instance blades, screws, cylinders, cylindroconical design. It was found that blades lead to fibrous tissue interposition, while screws and cylindroconical not;

1.2.4 The functional forces on dental implants

According to several authors [91, 34], the location and magnitude of the forces on all components of the bone-implant-prosthesis complex involve the correct distribution of stress and strain.

When an axial force is applied on natural teeth, tends to be higher at the temporomandibular joint (condyle) as seen in Fig1.5

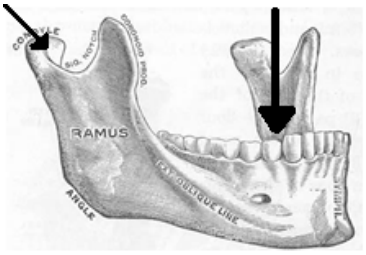

Figure 1.5: the arrow on the left indicates the point of the highest ([53])

However, typical values of axial forces are listed in the following table 1.1.

On the other hands, considering a biting force on a prosthesis, is not simple understand how the load reachs the bone-implant interface via the implant. In addition, stress and strains influence the bone remodeling process around the implant [90]. Moreover, during clinical loading of the implant, the direction of the forces are often eccentric with the consequence to generate reacting forces and bending moments in the bone [35]. Therefore, the stress transmitted to the implant depends on where the load is applied on the prosthesis [63].

Also the implant surface influences the distribution of stress and strains [64, 100]; in fact, if the surface is rough, the total area used to transfer loads to the bone increase, thus lower stress can be achieved close to the implant. Moreover, rough-surface provides better mechanical interlock with the bone [27]. While, implants with smooth surfaces causes debonding with the bone, which leads to bone resorption due to stress-shielding [100].

The bone surrounding implants is another factor that influences the distribution of loads; in fact, as mentioned above, the bone at the implant proximity can strongly vary based on age, sex, and jaw-bone position. If the implant is well osseointegrated, the mechanical behavior of the interface is improved, moreover, stress are reduced in denser bone [30].

Table 1.1: Loads on natural teeth and dentures supported by implant

([53])

Description	**Typical Values**	**Reference**
Vertical component of biting force in adults, averaged over several teeth	200-2440 N	Craig 1980 [96]
Vertical component of biting force in adults, molar region	390-880 N	Craig 1980 [96]
Vertical component of biting force in adults, premolar region	453 N	Craig 1980 [96]
Vertical component of biting force in adults, incisor region	222 N	Craig 1980 [96]
Vertical component of biting force in adults wearing complete dentures	77-196 N	Ralph, Colaizzi 1984 [123, 37]
Vertical component of biting force in adults with dentures supported by implants	42-412 N (median 143 N)	Carlsson and Haraldsson 1985 [45]
Lateral components of biting forces in adults	20 N	Graf 1975 [49]
Maximum contact stresses on teeth	20 MPa	Carlsson 1974 [46]

Finally, is helpful considering the stiffness of the natural teeth and the implant to understand the distribution of loads.

According to *Naert* [53] the values of the stiffnesses of dental implants and teeth. As we can see from the table 1.3, the stiffness difference between the implant and the natural teeth is one order. This is due to the absence of periodontal ligament, that with its elasticity, balances the

biting load on the surrounded bone.

Table 1.2: Stiffness for natural teeth and implants

([53])

Test condition	**Stiffness**	**Reference**
Branemark fixture (7 mm) plus abutment screw, abutment and gold cylinder. (Implant alone, no interfacial tissue)	4,55 N/μm	Hoshaw and Brunski 1988 [108, 63]
Branemark (7 mm) in trabecular bone (bovine tibial metaphysis)	2,50 N/μm	Hoshaw and Brunski 1988 [108, 63]
Branemark in plycarbonate plastic	3,66 N/μm	Hoshaw and Brunski 1988 [108, 63]
Natural teeth, human molar	0,1-1 N/μm	Richter et al 1990 [34]

1.2.5 Bone density classification

In the early 1970, *Linkow* identified three categories of bone density [18]:

1. class I: this type of bone consists of distribuited trabeculae with small cancellated spaces;
2. class II: the cancellated spaces are bigger with less uniformity of trabeculae;
3. class III: large cancellated spaces between trabeculae.

Linkow stated that Class III is related to higher risk of failure of dental implants.

In 1985, *Lekholm and Zarb* provided a scale based on four bone qualities [114]:

1. quality I: is composed of homogeneous compact bone;
2. quality II: is present a thick layer of compact bone surrounding dense trabecular bone;
3. quality III: the cortical layer become very thin surrounding an high-density trabecular bone;
4. quality IV: thin layer of compact bone surrounding a low-density trabecular bone.

Several studies tried to assess implant failure considering as unique variable the type of bone, reaching results which indicate that type III and IV are related to the most probable failure.

In the 1989, *Misch* proposed another classification system with four different bone density groups, based on the macroscopic cortical and trabecular bone characteristics [15, 16]. Considering both dense and porous cortical bone, both coarse and fine trabecular bone, can be listed the four categories:

1. D1 bone: is dense cortical bone (absent in the maxilla and rare in the mandible);
2. D2 bone: has dense-to-pouros cortical bone on the crest and, within the bone, has coarse trabecular bone (most common bone in the mandible, especially in the anterior, and sometimes present also in anterior maxilla);
3. D3 bone: has thin cortical layer and, within the bone, essentially fine trabecular bone (most common bone in anterior and posterior maxilla);
4. D4 bone: is the softest bone. Has not cortical crest with only fine trabecular bone (posterior maxilla).

The bone density can be assessed during surgical procedure by tactile sense, the general location in the mouth, or through radiography.

With the respect to Young modulus, *Misch et al* found different values for each bone density as listed in the following figure1.6

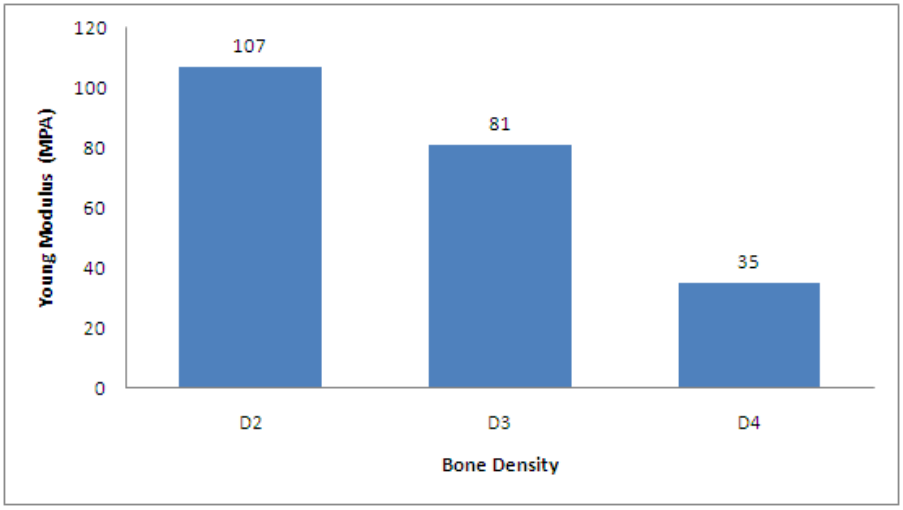

Figure 1.6: Elastic modulus for the different bone densities ([18])

Comparing these values with Young modulus of titanium (circa 100 GPa) *Misch et al* concluded that the difference between two materials may creates microstrain conditions of pathologic overload and cause implant failure. In fact, from this point of view, titanium-D1 bone interface exhibits very small microstrain difference than titanium-D4, which, is more likely to cause implant mobility and failure.

1.2.6 Implant success and failure

The huge development of implant dentistry brought to the need assessing health criteria in order to follow pre-established protocols which might lead to the best outcomes. Nowadays in literature, often, there are discordant and confuses opinions because classify each clinical case is hard. Nevertheless, is essential define a common criteria which allow more reliable considerations about the past, the present and the future

of the clinical dentistry. The criteria for success in implant dentistry are certainly complicated. In addition, several dental health criteria have been adpted for implants [17, 24], which are different from natural tooth, for instance, they do not decay, they do not have dental pulps to function as early indicators of pain and do not have periodontal membrane [18].

According to *Misch*, the general term success in implant dentistry should be replaced with the concept of quality of health, with a health-disease continuum describing the status of the implants[18]. In this prospective, *Misch et al* in 2007 at the International Congress of Oral Implantologists (Pisa, Italy), described the Implant Quality Scale in which they divided the management of dental implants which are classified in four levels [20], as reported in the following Tab1.5.

Table 1.4: Implant Quality Scale

Group	**Management**	**Clinical conditions**
I. Success (optimum health)	Normal maintenance	No pain or tenderness upon function; 0 mobility; No exudate history; less than 2 mm radiographic bone loss from initial surgery; Probing depth less than 5 mm;

II. Survival (satisfactory health)	Reduction of stresses; Shorter intervals beetween hygiene appointments; Gingivoplasty; Yearly radiograph	No pain; 0 mobility; 2-4 mm radiographic bone loss; Probing depth 5 to 7 mm; No exudate history
III. Survival (compromised health)	Reduction of stresses; Drug therapy (antibiotics, chlorhexidine); Surgical reentry and revision; Change in prosht-esis or implants	No pain upon function; 0 mobility; Radiographic bone loss $\geq 4mm$; Probing depth $\geq 7mm$; May have exudate history
IV. Failure (clinical or absolute failure)	Removal of implant	Any of the following: Pain upon function; Mobility; Radiographic bone loss $\geq 50\%$ length of implant; Uncontrolled exudate; No longer in mouth

As regard the failure, *Misch and Jividen* [40] classified implant failures as a function of the time:

- *surgical failure*: describes the failure due to the surgical procedure, for istance, fractures during the osteotomy, failure to obtain rigid fixation etc. etc;

- *osseous healing failure*: describes failure due to osseointegration process with the consequence of weak bone-implant interface;
- *early loading failure*: describes failure during the first year, in which the loads on the implant the osseous healing is compromised;
- *intermediate implant failure*: occurs at 1 year $\leq$ implant's life $\leq$ 6 years as a consequence of prosthesis function;
- *late implant failure*: occurs at 6 years $\leq$ implant's life $\leq$ 10 years of prosthesis loading;
- *long term failure*: $\geq$ 10 years of loading.

1.3 Implant stability

Implant stability and osseointegration are tightly related. In fact, osseointegration is influenced by the process of implant stability which is a measure of the clinical immobility of an implant [31, 61].

According to *Meredith* [84], the stability can be divided into primary and secondary as a result of healing time. Primary stability is achieved straight after surigcal procedure, and depends upon factors such as bone quality and quantity, surgical tecnique, implant geometry. Secondary stability depends on bone formation and remodelling [31, 61].

It has been shown that cortical bone thickness is one of the most important factors for primary stability and consequently the process of osseointegration [33, 52, 56]. In addition, *Tabassum et al.* reported that a thickness of 2mm is crucial to obtain primary stability [4].

Other studies focused on surgical tecnique because might damage the bone leading to failure of implants [77, 78].

Finally, *Vercaigne et al* have demonstrated that rough surfaces improve primary stability because enlarging area surface in contact with the bone [106].

1.4 Methods used to assess implant stability

The methods used to assess primary stability can be divided in destructive and non-destructive methods. Indeed, nowadays, an important study is on vibrational analysis, as periotest and resonance frequency analysis, because, if they are reliable tests, they may offer a non-destructive evaluation of dental implant stability.

1.4.1 Destructive methods

Reverse torque test

The reverse torque test, also called removal torque, was proposed by *Roberts et al* in 1984 [121]. This method can be considered destrutcive as to a counterclockwise (reverse) force with a computerized torque driver (figure 1.7), after predermination healing period until break bone-implant contact is applied.

Figure 1.7: Removal torque
([40])

Measuring the torque in N·cm, should provide the state of osseointegration in act. This test is mostly used in experimental studies because is misunderstood the threshold torque that involvee implant failure. In fact, a torque ranges between 10 to 20 Ncm should be tollerated by the

implant while if failing it is presumed to be fibrous encapsulated [40].

According to *Sullivan et al*, a primary objective of RTT is to identify nonintegrated implants at the earliest possible stage with a clinical verification method that is "objective, easy to administer, use available armamentaria, be as definitive as possible within the available knowledge base, and possess an adequate level of safety so that damage to the implantbone interface does not occur" [32]. Unfortunately, RTT is affected by several interpretations by clinicians as determination of bone density, of micromovements, the effects of implant size and design. From this point of view, since there are four type of bone according to either Leckolm and Zarb or Misch scale, a clinician has to understand what can be the bone density to applies the right torque avoiding the failure. Also integrated implant movement depends upon bone density, since the stiffness is dependent upon density [21]. Considering stress, *Herman et al* suppose that, as a consequence of torque, the stress transferred to the bone, lead to crestal bone loss [67]. Moreover RTT places a shear forces on the implant that is not the physiological loading, thus, it do not provide prognostic information, for instance, if bone-implant interface is able to support occlusal force [32].

Pull-out, push-out and push-in test

This class of tests are essentially the same, and consist of applying an axial force along the fixture until break the bone-implant interface. They produce forces in different directions as seen in figure 1.8. These types of test, as well as removal torque, are used to measure the strenght of bone-implant interface. Probably, they might be a good experimental choice to compare either different implant materials or coating methods, bone quality and quantity as to is expected they provide different strength with new bone formation. The pull out test was first introduced by *Bechtol* [8] in 1959 when he compared two different types of bone screw implant. Since then pull-out and push-out tests were used in several

experimental studies to assess the stability of the bone-implant interface [113, 107, 23].

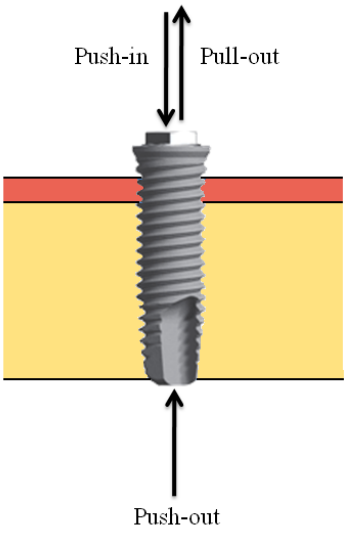

Figure 1.8: Directions of forces in pull-out, push-out and push-in tests

1.4.2 Non-destructive methods

Imaging techniques

Imaging techniques are widely used to assess both quantity and quality of the jawbone. They are used prior to surgery to estimate height and width of the bone, degree of the corticalisation, density of mineralisation and amount of cancellous bone. Following the surgery, imaging methods are used to assess the health of the implant, evaluating the bone quantity and quality changes, and estimating crestal bone loss, which is a consequence of the osseointegration process.

A large variety of imaging techniques are used in dentistry such as panoramic and intra-oral radiography, computer tomography, magnetic resonance imaging (MRI)[28]. Conventional radiography has poor capacity to predict less than 30-40% in changes of bone mineral [10] as well as trabecular bone loss. Indeed, to evaluate bone changes a three-

dimensinal technique is needed as they are more accurate, but, they are extremely costly, in addition, it should be noted that a follow up with such methods is not health.

The Periotest method

The Periotest is a commercial system (Siemens) based on the impact hammer method, in which a handheld rod is accelerated by an electromagnet and impacts the tooth (figure 1.9). The contact time is measured by an accelerometer incorporated into the head and the signal is analyzed; the response of the instrument is a number called "periotest value (PTV)" which gives information about the damping characteristics of tissues surrounding teeth or implants [118].

Figure 1.9: Periotest method
(Source: www.oral-implantology.blogspot.com)

The Periotest was introduced by *Schulte et al* to perform measurements of the damping characteristics of periodontal ligament (PDL), thus assessing mobility of natural tooth [119, 120]. When used to assess implant mobility, usually provides a range score from -5 to +5. It should be noted that for natural teeth, these values span from -8 to +50. Low score indicates low mobility, i.e. robust implant. [55]. However the sensitivity of this test to measure implant stability has been questioned [76] and, in addition, some implants may be falsely interpreted as well

integrated.

Neverthless, the Periotest was used considerably as method to assess implant mobility [73, 102, 6, 85, 58, 7], but the measurements are influenced by several factors, namely the distance from the striking point to the first bone contact [70, 85, 94], the position on which the Periotest impacted on the abutment [55, 58, 59, 60]; in addition, regarding the effect of bone density, no linear correlation was found with the PTV [102, 101]. Therefore the reliability of this method is questionable because of poor sensitivity, susceptibility to many variables [84, 47].

Resonance frequence analysis

Meredith et al introduced a method based on resonance frequency analysis (RFA) [84], that employs a small L-shaped trasducer screwed to the implant or abutment (figure 1.10).

Figure 1.10: Resonance frequency analysis method ([3])

The trasducer is excited by a sinusoidal signal tipically ranging between 5KHz and 15KHz. The stability of the implant is indirectely determined through the value of the first reasonance peak, therefore, theoretically higher is resonance frequency more stable is the implant. The reasonance peak is converted in a value, called "implant stability quotient (ISQ)", from 0 to 100. The higher the value the greater the

stability. Although there is not established treshold level, practitioners consider values below 45-50 risky for the implant stability [44]. To date, two commercial systems based on RFA are clinically used namely Ostell (Integration Diagnostic) and Implomates (Biotech). Using RFA, various authors have concluded that ISQ value increases after implant insertion, as consequence of the more stable bone/implant interface [86]; in addition, the increased value is particularly evident for the soft bone [97, 95, 5].

Considering implant design, *Boronat et al* [1] concluded that ISQ values are not related to implant length or diameter, but the effective implant length, which represents the sum of the abutment length and exposed implant threads. EIL influence RF, in particular, has been shown to be inversely proportional to the level of RF. On other hand, *Ostman et al* proved that length of implant influences RF [92], in particular a lower ISQ is observed with longer implant.

The feasibility and reliability of the RFA method have been investigated recently. *Huwiler et al* [81] focused on figuring out if RFA might have predicted the loss of stability with low score; in fact, the loss of stability was coincidental with low ISQ but could not not be predicted. According to *Meredith* [83, 84], for the implants which shows low stiffness, the first resonance peak could not be identified, and consequently, only the second peak that provided an higher ISQ value. *Nedir et al* [95] after a study conducted in 2004, believed that the RFA method reflects only the stiffness of the implant-bone interface. Hence, at the present time, RFA seems to be questionable and therefore, is preferable to conduct longitudinal studies associating ISQ value with histological studies.

In conclusion the table 1.6 provides an outlook of such techniques.

Table 1.6: Implant stability methods

Test	**Features**	**Benefits**	**Drawbacks**
Reverse torque	Applying a torque until break bone implant interface	Reliable Easy to use Strength of the bone implant interface	Destructive Only post-sirurgical evaluation Difficult clinical use
Push out, push in and pull out	Applying a directional force until break bone implant interface	Reliable Strength of the bone implant interface	As reverse torque
Imaging techniques	Rapresention of an object by means of an image	Non desctructive Can be used pre and post surgery	Bulky Costly
Periotest	Modal analysis by means of impact hammer method	Non destructive Pre and post surgical evaluation Clinical use	Influenced by several factors such as implant geometry Low sensitivity
Resonance frequency analysis	Modal analysis by means of piezo trasducers	As periotest	As periotest

1.5 The Electro-Mechanical Impedance Method

The EMI method is a non destructive technique used primarily in the field of civil engineering, such as buildings, bridges, dams, wind turbine systems etc etc, as structural health monitoring system (SHM). The

SHM system is a very important process which implements a damage detection strategy in order to prevent catastrophic disasters. According to *Ciang et al* [14], the SHM involves the observation of a system over time using periodically sampled dynamic response measurements from an array of sensors. the extraction of damage-sensitive features from these measurements and the statistical analysis of these feauteres to determine the current state of structural health. In this context the damage is view as the change of structural integrity such as changes of material properties and/or geometrical properties [25].

EMI background

This EMI method utilizes the electro-mechanical impedance of piezoelectric materials, which is directly related to the mechanical impedance of the host structure. Therefore, the presence of damage can be detected by the variations of the PZT electrical admittance (the inverse of impedance), in particular, frequencies and conductance shifts from the undamaged signature.

Piezoelectric materials can work as both sensors and actuators. In fact, in the presence of voltage (or electric charge), they provide a force; in the same way, a force applied on the material, cause a electrons flow.

In the electrical impedance method, the piezoelectric ceramic Lead Zirconate Titanate (PZT) are coupled to the monitored structure. Applying a voltage, typically 1V in the kHz range, the PZT start to vibrates transferring its vibrations to the host structure. Simultaneously, the structure's vibrations, influence the electrical admittance of the PZT, which is read by impedance analyzer. Any change of structural characteristics such as stiffness, damping, mass distribution, would influence the reading electrical admittance. Plotting the conductance (the real part of admittance) as a function of frequency shows informations about the health state of the structure.

Several papers are reported on literature proving the reliability and

effectiveness of method detecting structural damage [68, 42, 41, 13, 115]. Nevertheless, its use in biomedical fields is rather limited. *Bhalla and Bajaj* characterized the healing process of a fractured bone using PZTs [105]. *Bender et al* monitored capsule formation around soft tissue implants [69]. The use of piezoelectric wafer active sensors and EMI method in rats' spine was instead reported by *Giurgiutiu et al* [117].

PZT-Structure interaction model

Since the birth of the EMI technique, several authors reported mathematical modeling of PZT trasducers coupled with the structure, for instance, *Liang et al* in 1994 [9], presented 1D coupled electro-mechanical model, while *Bhalla and Soh* developed 2D and 3D interaction models [104].

In this section the 1D model is presented.

The constitutive relations for piezoelectric materials under small field condition are [57]:

$$\begin{bmatrix} D \\ S \end{bmatrix} = \begin{bmatrix} \overline{\varepsilon^T} & d^d_{im} \\ d^c_{jk} & \overline{s^E} \end{bmatrix} * \begin{bmatrix} E \\ T \end{bmatrix} \tag{1.1}$$

[D] (C/m^2) is the electric displacement vector of size (3×1), [S] is the dimensionless strain tensor of size (6×1), [E] (V/m) is the applied external electric field vector of size (3×1), and [T] (N/m^2) is the stress tensor of size (6×1). $[\overline{\varepsilon^T}]$ (F/m), is the dynamic dielectric permittivity tensor of size (3×3) under constant stress, $[d^d_{im}]$ (C/N) is the piezoelectric strain coefficient tensors of size (3×6) for the direct effect, while, $[d^c_{jk}]$ (m/V) of size (6×3) for the converse effect, $[\overline{s^E}]$ (m^2/N) is the dynamic elastic compliance tensor under constant electric field of size (6×6). In both $[d^d_{im}]$ and $[d^c_{jk}]$ the first subscript indicates the direction of the electric field and the second the direction of mechanical strain.

The mechanical impedance of the structure is defined as the ratio of the force to the velocity at the point of the application of the force:

$$Z = F/u_0 \tag{1.2}$$

where it is modelyzed as a spring-mass-damp system given by:

$$Z = c + j\left(m\omega - \frac{k}{\omega}\right) \tag{1.3}$$

where c is the damping factor, ω is the excitation frequency, m is the mass and k is the spring constant.

The interaction model is described in the following Figure 1.11.

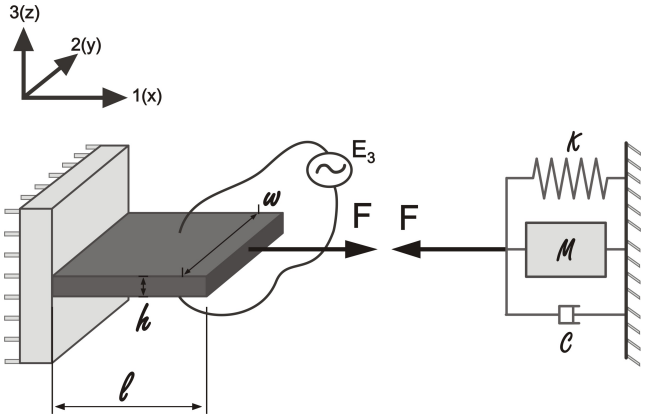

Figure 1.11: PZT-structure model

Therefore, considering the electric field in direction 3 and the mechanical strain in direction 1, the Eq.(1.1) can be re-written as:

$$D_3 = \overline{\varepsilon^T}_{33} E_3 + d_{31} T_1, \tag{1.4}$$

$$S_1 = \frac{T_1}{\overline{Y^E}} + d_{31} E_3, \tag{1.5}$$

where S_1 is the strain in direction 1, D_3 the electric displacement over the PZT transducer in direction 3 and T_1 is the axial stress in direction 1. $\overline{Y^E}$= $Y^E(1+\eta j)$ is the complex Young's modulus of elasticity of the PZT transducer at constant electric field and $\overline{\varepsilon^T}_{33}$=$\varepsilon^T_{33}(1-\delta j)$ is the complex electric permittivity of the PZT transducer at constant stress. η and δ are the mechanical loss factor and the dielectric loss factor

respectively of the PZT transducer.

Liang et al [9] reported the following differential equation regarding the vibration of the PZT trasducer:

$$\overline{Y_{11}^E}\frac{\partial^2 u}{\partial x^2} = \rho\frac{\partial^2 u}{\partial t^2} \tag{1.6}$$

where u is the displacement at any point on the patch in direction 1. The equation can be resolved by the method of separation of variables obtaing:

$$u = (A\sin\kappa x + B\cos\kappa x)e^{j\omega t} \tag{1.7}$$

where κ is the wave number defined as: $\kappa{=}\omega\sqrt{\rho/\overline{Y^E}}$.

To obtain the constant A and B the first boundary condition is that at x=0, u=0 yields B=0.

Hence, the strain in the PZT and the velocity are:

$$S_1 = \frac{\partial u}{\partial x} = Ae^{j\omega t}\kappa\cos\kappa x \tag{1.8}$$

$$\dot{u}(x) = \frac{\partial u}{\partial t} = Aj\omega e^{j\omega t}\sin\kappa x \tag{1.9}$$

From the eq 1.5 substituting the expression and the strain obtained, the constant A can be derived as:

$$A = \frac{Z_a V_o d_{31}}{h_a\kappa\cos\kappa l_a(Z + Z_a)} \tag{1.10}$$

where Z_a is the short-circuited mechanical impedance of the PZT transducer:

$$Z_a = \frac{\kappa w_a h_a\overline{Y^E}}{(j\omega)\tan\kappa l_a} \tag{1.11}$$

This is defined as the force needed to produce unit velocity in the PZT transducer in short circuited condition (i.e. ignoring the piezoelectric effect) and ignoring the host structure. The electric current which is the

time rate of change of charge can be obtained as:

$$\overline{I} = \int\int_A \dot{D}_3 dxdy = \jmath\omega \int\int_A D_3 dxdy \tag{1.12}$$

Making use of the PZT constitutive relation, and integrating over the entire surface of the PZT transducer (-1 to 1), we can obtain the expression for the electrical admittance as:

$$\overline{Y} = G + jB = 2\omega j \frac{wl}{h}\left[\left(\overline{\varepsilon_{33}^{T}} - d_{31}^{2}\overline{Y^{E}}\right) + \left(\frac{Z_a}{Z+Z_a}\right) d_{31}^{2}\overline{Y^{E}}\left(\frac{\tan\kappa l}{\kappa l}\right)\right] \tag{1.13}$$

Assuming that the mechanical property of the PZT does not change during the monitoring period, equation 1.13 shows that the electrical admittance is related to the mechanical impedance of the structure, hence, any change of structural properties provide different values of the admittance. The electrical conductance which is the real part of the admittance is typically used for structural monitoring as it is more reactive to changes occurring in the host structure.

Aim of the experimental study

The experimental study has been conducted mostly at University of Pittsburgh in the laboratory of Non Destructive Evaluation (NDE) at the department of civil engineering.

Evaluation of dental implant stability is one of the most important factor leading to implant success. Moreover, during last two decades non destructive methods became extremely spread. Nevertheless, several studies, as reported in the previous sections, questioned the feasibility and reliability of such methods, for instance, the Periotest and the Resonance frequency analysis.

In this experimental study, the electro-mechanical impedance method (EMI) has been preliminary utilized to assess dental implant stability. This technique comprised the use of a piezoelectric trasducer bonded at the top of dental implant; measuring the electrical admittance of the trasducer information about the stability is given. Hence, such method might be a potential way by means of a clinician determines both the current and further implant healthy conditions.

Furthermore, a consequence use for different biomedical devices is elicited.

Chapter 2

Materials and Methods

In this study two series of tests were implemented to evaluate the effectiveness of EMI for monitoring bone-interface stability properties vs healing time:

i Tests simulating the inverse of the healing process.

ii Tests simulating healing process.

The first series comprised the use of solid rigid polyurethane foam from Sawbones®, which is widely used to simulate the human cancellous bone. Foam specimens were dissolved by means of nitric acid and the decomposition process was monitored by measuring the EMI of PZTs attached to implants embedded in the foam.

In the second series the implants with attached PZTs were embedded inside a long specimen made of fresh joint compound specimen.

It is shown that the EMI is a viable method for the noninvasive and nondestructive evaluation of dental implants.

Compression test of the hard polyurethane, i.e. 40 pcf, were conducted in order to correlate the loss of mechanical properties of the foam to the electro-mechanical signatures obtained with LCR meter.

2.1 Materials

In this study two types of implants, namely CORE with internal hexagon and PLUS with external hexagon from Bio Implant (Italy), were used. One implant type, hereafter indicated as the short implant, was 2.9 mm in diameter and is 10 mm high. The second type of implant, hereafter indicated as the long implant, was 5 mm in diameter and 15 mm high. The implants were entrenched in three different materials, namely Solid Rigid Polyurethane Foam (40 pcf), Cellular Rigid Polyurethane Foam (10 pcf), and a commercial joint compound. The foams were both from Sawbones® and they were respectively high-density polyurethane 640 Kg/m^3 (40 lb/ft^3), low-density polyurethane 160 Kg/m^3 (10 lb/ft^3) and joint compound.

The densities of the polyurethane foams were chosen as they are representative of two bone densities, according to the classification D1, , D4 proposed by Misch (1989,1990). The hard (denser) polyurethane can be related to a D1 bone, while the soft polyurethane can be considered representative of a D4 (softer) bone.

The transducers' admittance was measured by means of an Agilent E4980A LCR meter connected to a multi-channel Agilent 34970A Data Acquisition Switch Unit. Both were controlled through a Visual Basic Application interface. Following up preliminary tests, the measurements were taken in the frequency range 0-1 MHz at 0.5 kHz interval. This interval is dictated by the best resolution achievable by the instrument.

2.1.1 Sensors

Piezoceramics PSI-5A4E transducers from Piezo Systems, Inc. were used. They were custom cut to be circular (3.175 mm diameter and 0.1905 mm thickness) and square (1×1×0.267 mm) and (2×2×0.267 mm) elements.

As described in the previous chapter, the EMI method comprises

the use of a piezoceramic transducer which acts as both sensor and actuator. In addition they have other advantages such as compactness, sensitivity over large strain bandwidth and ease of embeddability for performing structural health monitoring [57]. The PZT sensors used in this experimental study consist in Lead Zirconate Titanates (PZTs) which are solid solutions of lead zirconate and lead titanate, often doped wit other elements to obtain specific properties. The sensors are manufactured by mixing together lead, zirconate and titanium oxide powders and heating around 800-1000°C. During the cooling process, the material undergoes to a paraelectric to ferroelectric phase transition and the cubic unit cell becomes tetragonal. Applying an electric field on his thickness the unit cells align to the direction of the applied field. This process is called poling and imparts a permanent net polarization to the ceramic. Therefore, in this state the material shows both the direct and converse piezoelectric effect [57].

Since these transudcers are ceramics they provide high elastic modulus, low tensile strength, and brittleness.

2.2 Methods

2.2.1 Mechanical test

Uniaxial compression tests were performed according to UNI 6350-68 by using a uniaxial electromechanical system (Instron model 4200, load cell 1 kN). Cylindrical specimens (diameter = 12 mm, h = 12 mm) were punched out from a slice of high density foam and immersed in a solution of nitric acid [w/w] = 68-70% for up to 12 hours. At each time point, foam specimens were taken from the solution and exsiccated at ambient temperature until constant weight. Specimens have then tested at 1 mm min^{-1} crosshead rate, performing one loading/unloading cycle up to = 50% or up to the maximum deformation allowed by the load cell.

2.2.2 Test 1 and 2: inverse bone healing simulation

In the first two experiments the inverse process of bone-healing was simulated via degradation of the polyurethane foams. In the first test (Test 1) two different dental implants screw were placed in a 40×40×15 mm3 high-density foam. A square PZT (1×1×0.267 mm) was glued on top of the long implant while a circular PZT was glued on top of the short implant.

A scheme of the test specimens are presented in figure 2.1.

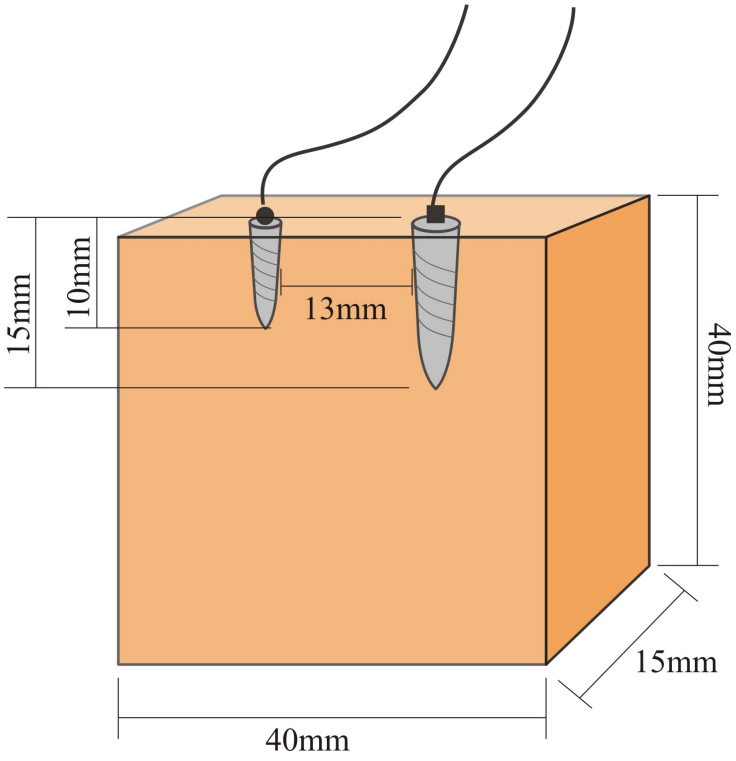

Figure 2.1: Polyurethane specimen

The foam was then immersed in a glass container partially filled with a solution of nitric acid ([w/w] = 68-70%). Measurements were taken every 30 minutes for 12 hours. The conductance and susceptance signatures during the monitoring period were compared to the baseline signature, which was taken at the beginning of the experiment immediately after immerging the sample into the acid, i.e. at 0 hours. The

baseline signature might be interpreted as the thoroughly healed bone as well as the level of full stability reached by the dental implant.

A similar procedure was conducted to monitor the degradation process in a 40×40×15 mm3 low-density foam (Test 2). The geometry of the specimen and the relative position of the CORE implants were the same as for Test 1.

For both experiments a preliminary measurement was conducted to evaluate the influence of the amount of liquid surrounding the specimen. In this pre-test the glass container was progressively filled with water and the values of G and B were measured. The test showed that the boundary conditions barely affect the electromechanical response of the transducer. Therefore it was concluded that any evaporation of the acid during the monitoring period would not affect the response of the transducers.A typical setup of the experiment with the polyurethane is shown in figure 2.2.

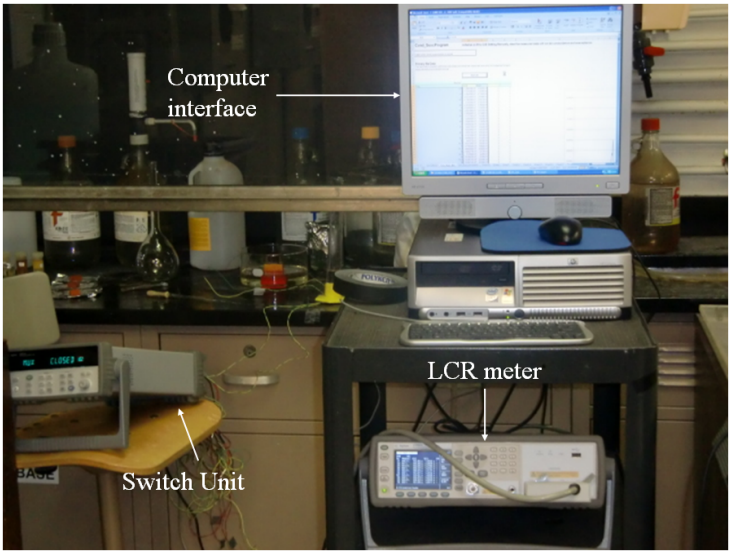

Figure 2.2: Experimental setup

2.2.3 Further decomposition test

For completeness, aa further decomposition test by means of nitric acid was conducted with the aim to evaluate the influence of the implant geometry on the electro-mechanical admittance. In fact, two PZT sheets with the same size, namely square (2×2×0.267 mm) were used. The main features, as the frequency shift and the RMSD are presented in the discussion chapter.

2.2.4 Test 3:Direct bone-healing simulation

In order to simulate the use of EMI during the healing process following surgical procedure a third experiment was conducted. A 125 mm long, 50 mm wide and x 20 mm deep specimen made of commercial joint compound (Gypsum Company, Chicago, US) was build. After the compound was set, four holes were created to accommodate the two types of implants used in this research. On top of all implants a square PZT (2×2×0.267 mm) was attached. The implants were then inserted into the holes and stabilized with fresh compound. The figure 2.3 illustrates the PZT-implant-compound system investigated during this third test. Longer implants are indicated as element 1 and 3 while the smaller implant occupied the 2nd and the 4th hole. Measurements during setting

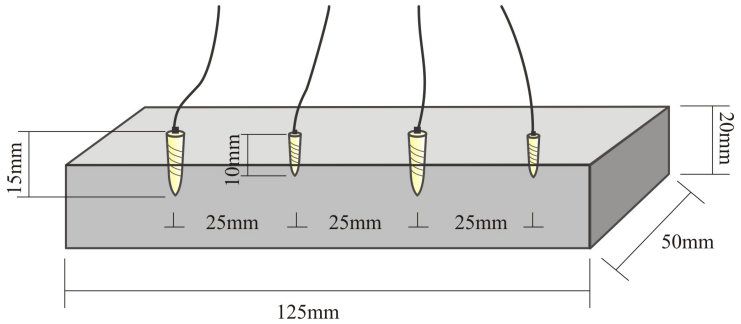

Figure 2.3: Joint compound specimen

process were taken at regular intervals.

Overall the table 2.1 summarizes the experimental procedure adopted

to monitor the stability of dental implants.

Table 2.1: Summary of the experimental procedure

Test#	**Specimen**	**Implant**	**Acid%**	**PZT**	**Monitoring time**
1	Hard polyurethane	Short	68-70 %	Circular	12 hours
		Long		Square	
2	Soft polyurethane	Short	68-70 %	Circular	12 hours
		Long		Square	
3	Joint Compound	Short	//	Square	216 hours
		Long		Square	

2.3 EMI frequency range

The typical frequencies used with the EMI method comprises a range between 30 and 400 kHz; in fact, according to *Park et al* [41], the wavelength of the travelling wave of any excitation should be smaller than the characteristic length of the damage to be detected in order to assure the best sensitivity of the test. Higher the frequency smaller is the area interrogated. Hence using higher frequency make the EMI method less sensitive to the boundary condition changes during the measurements. In addition a frequency range which shows 20-30 peaks is usually chosen since it implies an higher dynamic interaction with the structure.

Nevertheless, in this experimental study, a frequency range between 0 and 1 MHz was chosen to include the resonance peak of the transducer as well. In fact, this investigation is somehow different from the typical use of the EMI method. Moreover, an experimental study [117] found in literature shows the use of piezoceramic transducer to monitor, through the electrical admittance, the body reaction to implants; they used large frequency ranges, more than 2MHz.

2.4 Signal processing

To compare the impedance signatures changes, the root mean square deviation (RMSD) scalar damage metric was used. This metric use difference of the impedance at each frequency in calculating a scalar metric. First, the baseline metric related to the undumaged structure was taken. Then, the baseline was compared to the next measurements assessing the differences in act.

The RMSD is given by the following equation:

$$RMSD(\%) = \left(\sum_{i=1}^{n} \sqrt{\frac{[G_j(\omega i) - G_0(\omega i)]^2}{[G_0(\omega i)]^2}} \right) \times 100 \tag{2.1}$$

where $G_j(\omega i)$ is the conductance value of $\imath th$ frequency point of the $\jmath th$ decomposition time and $G_0(\omega i)$ is the baseline conductance value of the $\imath th$ frequency point, n is the upper limit of frequency range.

It has been shown that the RMSD is a reliable statistical method to evaluate the structural damage.

Finally, in this study the root mean square (RMS) was also computed which is given as:

$$RMS = \left(\sum_{i=1}^{n} \sqrt{\frac{G_j(\omega i)^2}{N}} \right) \tag{2.2}$$

where $G_j(\omega i)$ is the conductance value of $\imath th$ frequency point of the $\jmath th$ decomposition time and N represents the upper limit (i.e. in a range comprising of N frequencies).

Chapter 3

Results

3.1 Test 1: hard polyurethane (40 Kg/m^3)

The specimen during the decomposition time shows a dark red color and a partially mass loss as shown in figure 3.1.

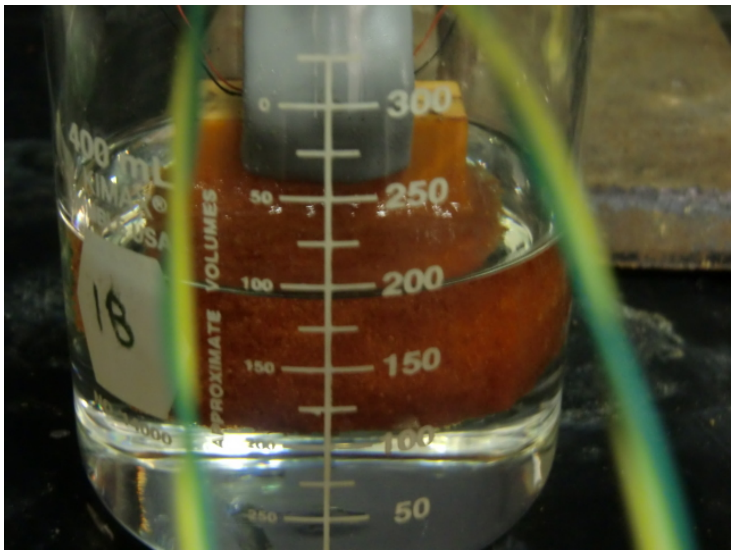

Figure 3.1: Polyurethane specimen during decomposition process

Figure 3.2a and 3.2b shows the conductance and the susceptance as a function of the frequency associated with the circular PZT. The results refer to four acquisitions, namely the baseline and after 2, 6, and 12

hours. The plots of the conductance are overlapped to the signature of the free PZT. For clarity the values of this signature are reported on the right vertical scale. The conductance signature shows two main peaks at about 700 kHz and 800 kHz. Overall the amplitude of both peaks decreased as the degradation progressed and therefore these amplitudes can be associated with the damping characteristics of the system. Outside the peak frequency ranges, i.e. below 600 kHz and above 820 kHz, the values of the conductance increased as the decomposition of the polyurethane progressed.

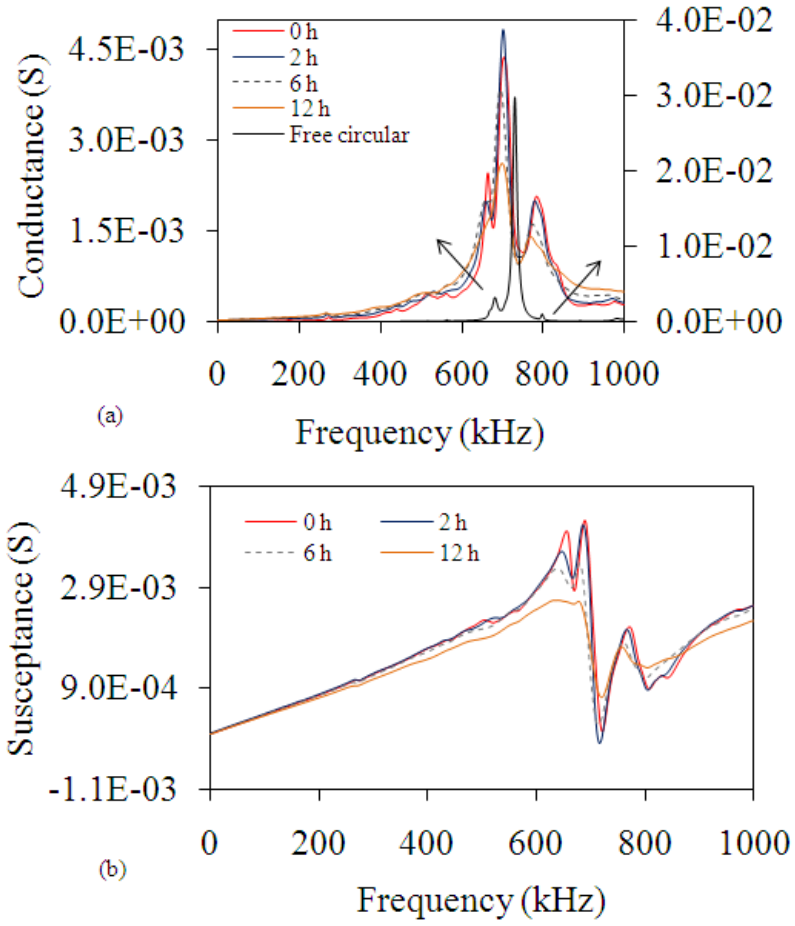

Figure 3.2: Test 1. Short implant: conductance (a) and susceptance (b) as a function of frequency.

It should be noted that the free PZT signature refers to the measure-

ment of the admittance without any structure coupling, namely PZT-air interface. In other words this signature would be the admittance value of equation 1.13 considering the impedance of the structure (in the equation Z) equal to 0. With the respect to the susceptance a decrease of the amplitude is observed.

A close up view of the conductance at lower frequencies is shown in figure 3.3 which shows a peak at 289 kHz. In this frequency range the increase of the conductance is evident.

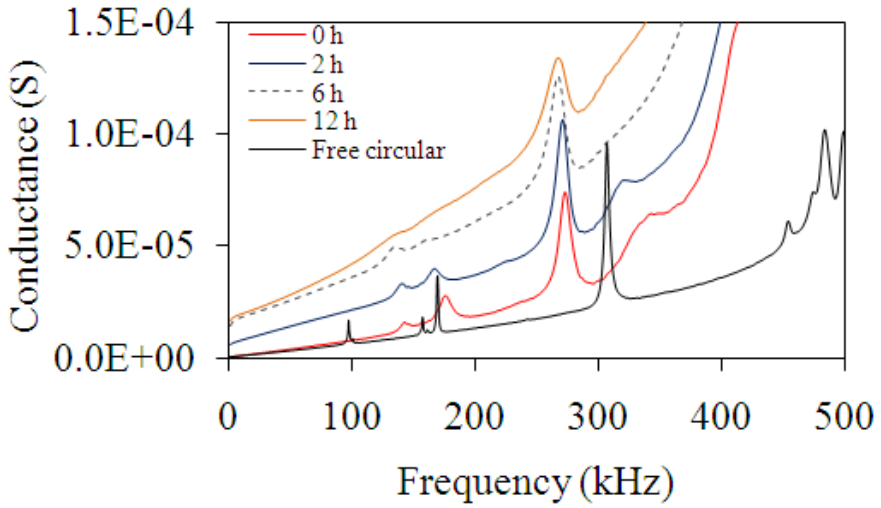

Figure 3.3: Test 1. Short implant: conductance as a function of frequency in the range 0-500 kHz.

The real and the complex component of the square (long implat) PZT admittance are presented in figure 3.4a and 3.4b respectively. The figures show two main peaks at 800 kHz and 900 kHz due to the resonance characteristics of the piezoelectric. At lower frequencies other 2 peaks are visible, namely at 380 kHz and 550 kHz; these peaks, as shown in figure 3.4c, reflect the increase of the conductance, in addition, the peaks become wider due to the damping characteristics of the system.

By comparing the response from the short implant, the response of the long implant shows smaller variation; these results suggest that, as expected the EMI method might be influenced by implant geometry.

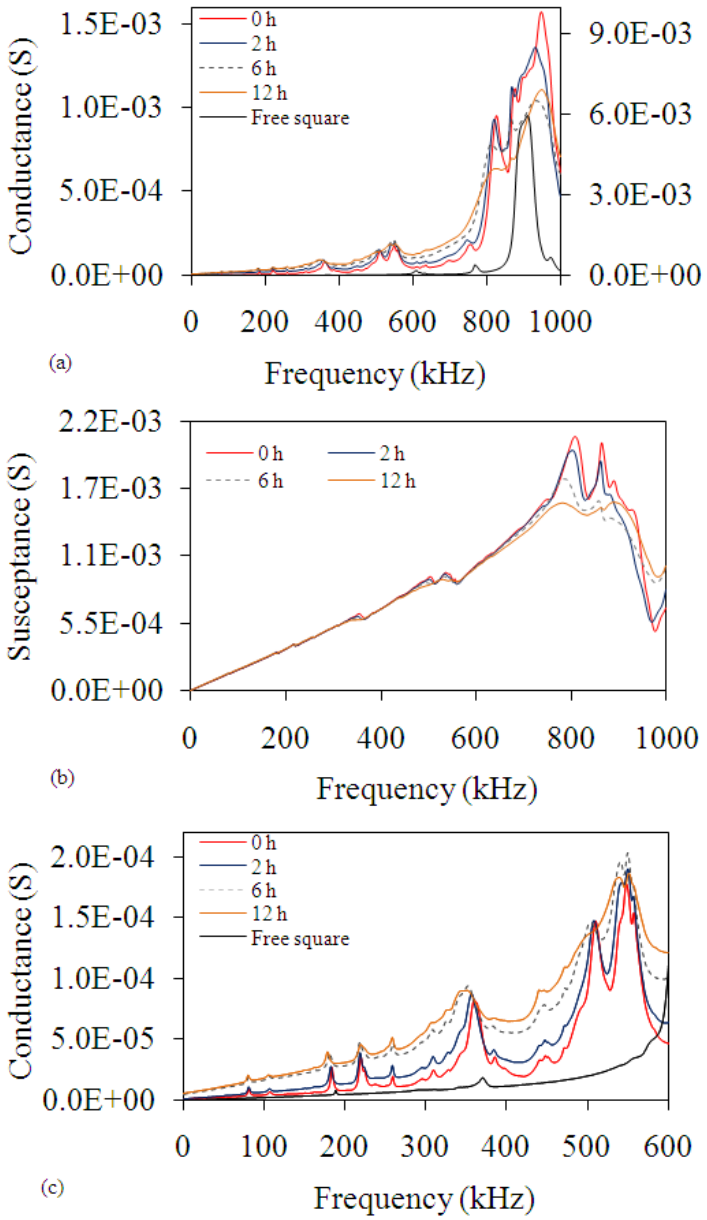

Figure 3.4: Test 1. Long implant: conductance (a) and susceptance (b) as a function of frequency and close up view of the conductance between 0-600 kHz.

To quantify the shift of the conductance frequency peaks observed in figure 3.4, the value of the frequency peak as a function of monitoring time is presented in figure 3.5a and 3.5b for the circular and 3.6a and 3.6b for the square PZT, respectively.

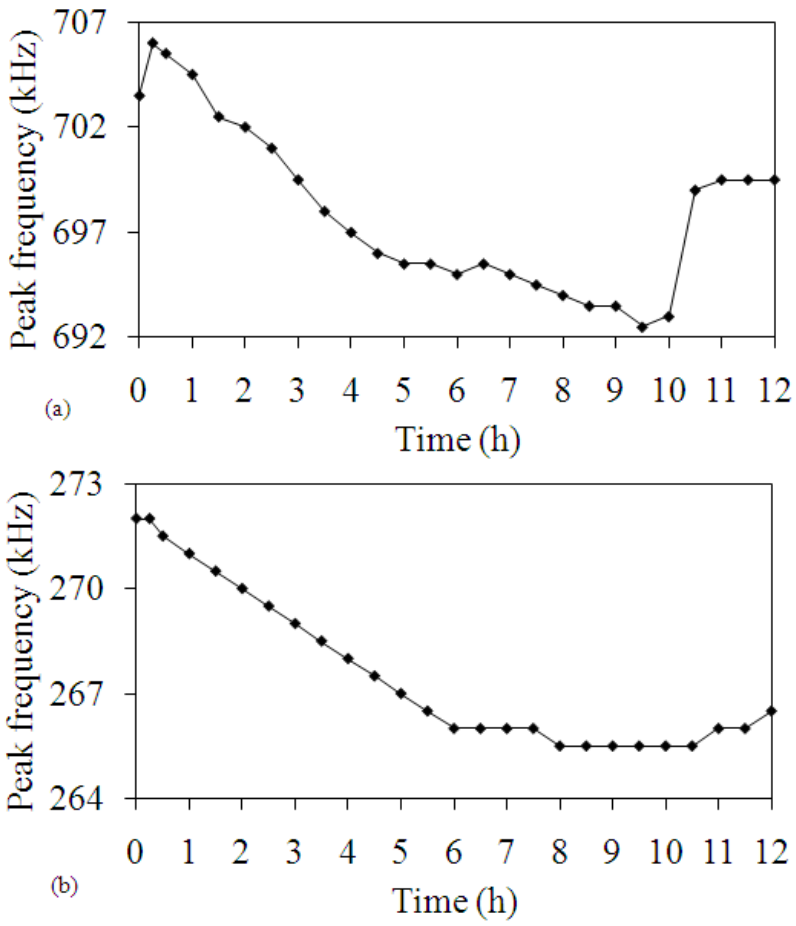

Figure 3.5: Test 1. Peak frequency for short implant around 700 kHz (a) and 270 kHz (b).

For the short implant a monotonic decrease of the peak frequency for the first ten hours is visible. The same cannot be said for the long implant where a parabolic behavior is observed around 900 kHz.

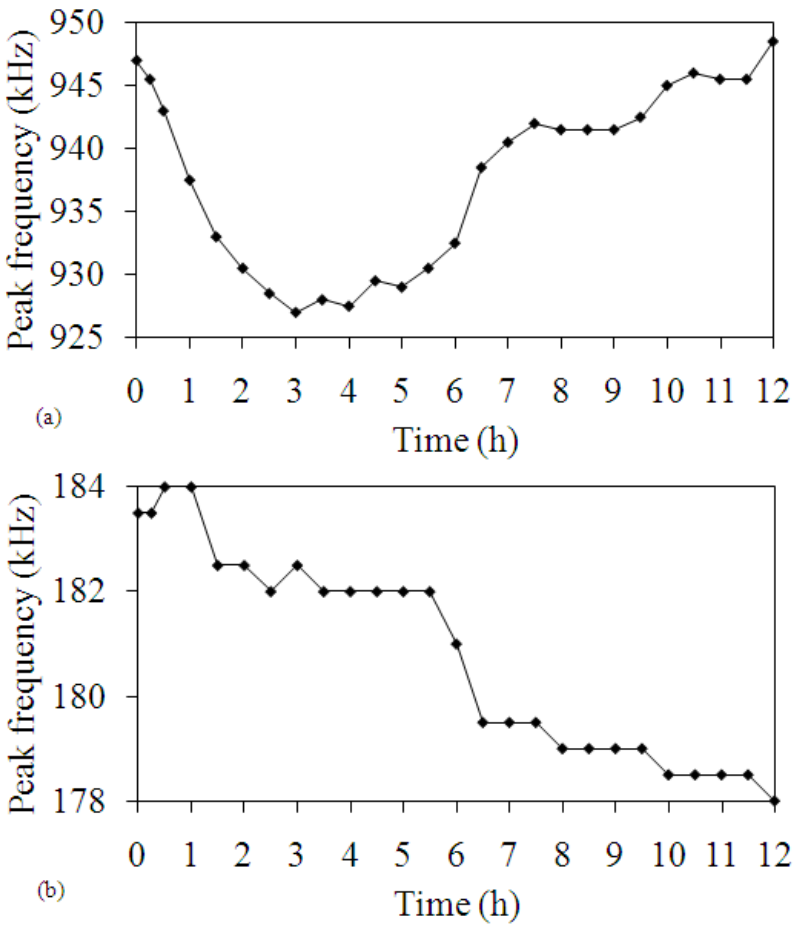

Figure 3.6: Test 1. Peak frequency for long implant around 900 kHz (a) and 180 kHz (b).

With the respect to statistical indices to analyze the extensive experimental data, as expressed in the second chapter the RMSD and RMS was reported in this study. The root mean square deviation (RMSD) of the conductance as a function of the monitoring time for both PZTs is illustrated in figure 3.7. For the first 6 hours both show the same trend. Then the RMSD associated with the square PZT presented a plateau. A 5% divergence is visible around 10 h.

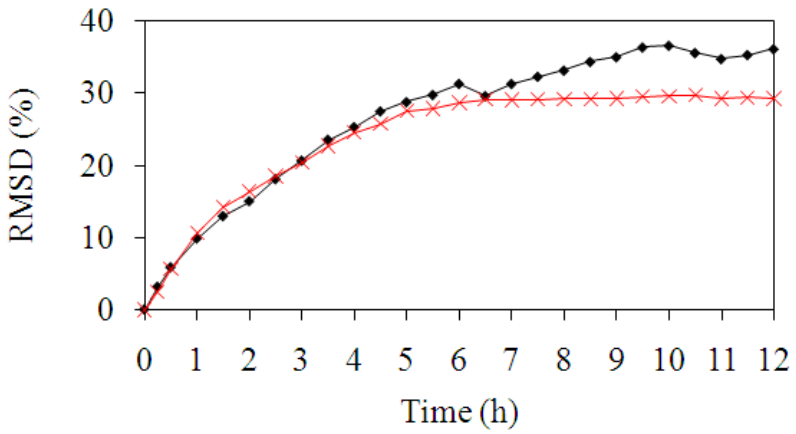

Figure 3.7: Test 1. RMSD for short (dots) and long (x) implant as a function of time.

The values of the root mean square (RMS) of the conductance over the 0 - 1000 kHz range normalized with respect to the baseline data are presented in figure 3.8 as a function of the monitoring time.

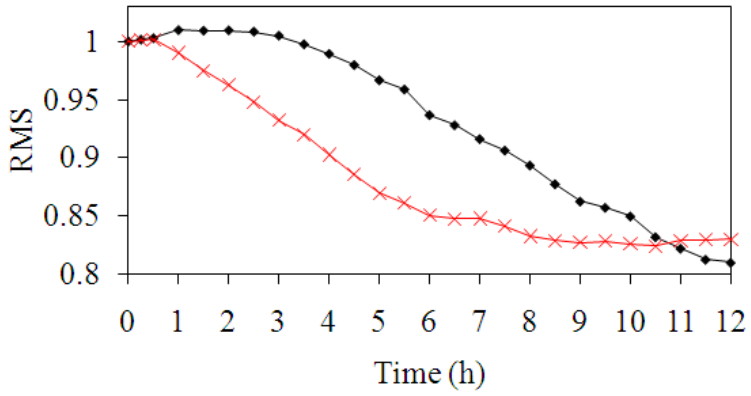

Figure 3.8: Test 1. RMS (normalized to the initial value for short (dots) and long (x) implant as a function of time.

The difference between the two PZTs is evident, although for both of them a monotonic decrease is visible.

In order to quantify the response of the structural impedance with respect to the monitoring time, the response of the conductance at every actuation frequency was considered. Figure 3.9a shows such a response at 705 kHz for the short implant and figure 3.9b at 825 kHz for the long

implant.

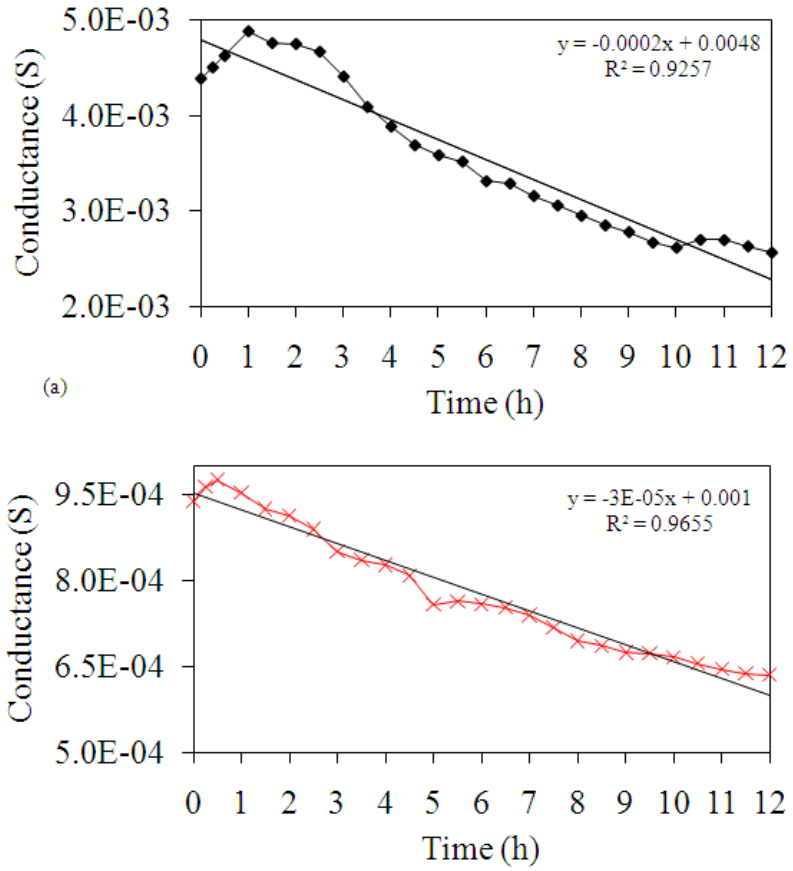

Figure 3.9: Test 1. Conductance at 705 kHz for the short implant (a) and at 825 kHz for the long implant (b) as a function of time.

A linear relationship between the conductance and the time t is assumed, and a mathematical relationship can be formulated as:

$$G(t, f) = m(f)t + C(0, f) \tag{3.1}$$

where G(t,f) represents the conductance at frequency f and time t, and m(f) is the gradient that is used to quantify the sensitivity of the conductance. It should be noted that Eq. 3.1 is an assumption based on the hypothesis that the physical degradation of the structural impedance is linearly proportional to the exposure time to the acid. For every fre-

quency, the slope was computed.

The values of these slopes as a function of frequency in the range 0-1 MHz are presented in figure 3.10. Positive slopes indicate that the conductance increases with time, i.e. with degradation. The variation of the slope values was larger in the range 600 - 820 kHz with a large negative peak at 705 kHz for the short implant and 825 kHz for the longer one. The fluctuations visible in this range are related to the shifts of peaks and valleys, which are, in turn, associated with the variation of the mechanical impedance of the structure.

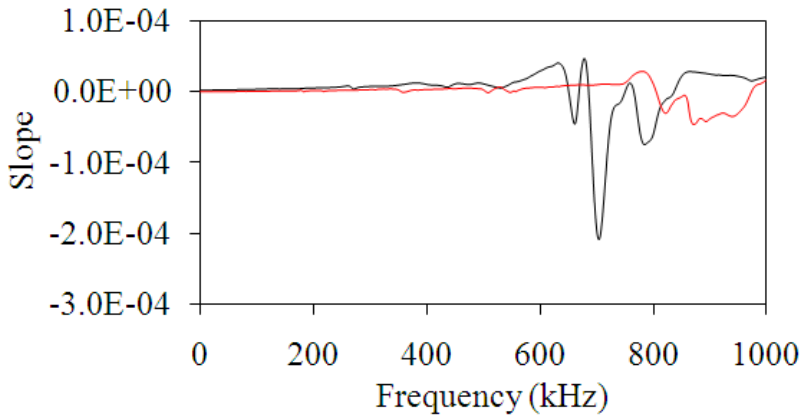

Figure 3.10: Test 1. Slope as a function of frequency for short (black line) and long (red line) implant.

The linear relationship between the conductance and the monitoring time reflects the degradation of the stiffness of the specimen, as demonstrated through the mechanical tests executed. The maximum slope, i.e. the largest sensitivity of the conductance to the degradation phenomenon, occurred at the resonance peak, which therefore might be exploited to assess the stability of the implant. The positive gradient in figure 3.10 implies that the conductance amplitude increases as the degradation progresses, while negative slope means that the conductance amplitude decreases as increasing the time.

3.2 Test 2. Soft polyurethane (10 Kg/m^3)

With the second test, the capability of the EMI method to assess the soundness of implants in soft bones was evaluated. The density of the polyurethane specimen used in this test is considered to be related to D4 soft bone, which has an elastic modulus of 35 MPa [18].

The conductance and the susceptance for the short implant is presented in figure 3.11, whereas figure 3.12 refers to the long implant. The

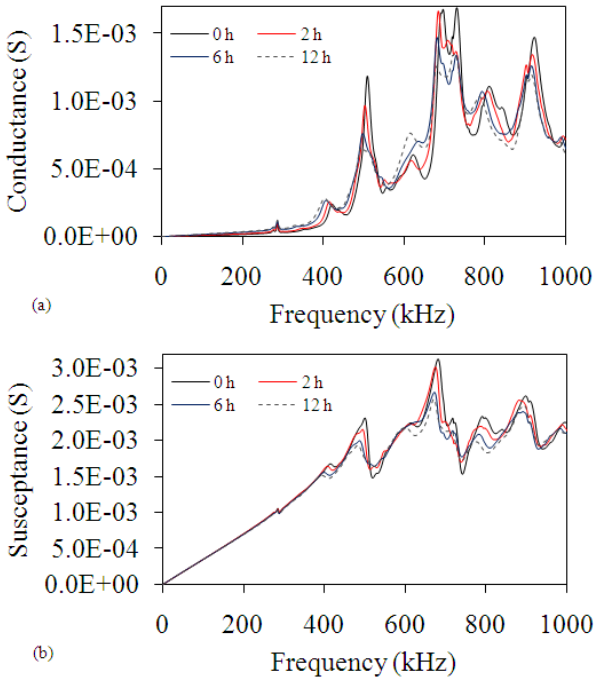

Figure 3.11: Test 2. Short Implant: conductance (a) and susceptance (b) as a function of frequency

responses observed in these figures are similar to the hard polyurethane, i.e. an increase of the conductance at frequencies outside the peak resonance ranges, and a decrease of the peaks amplitudes due to increase of damping. The same can be said for the susceptance, namely a decrease of the signature outside the resonance peak.

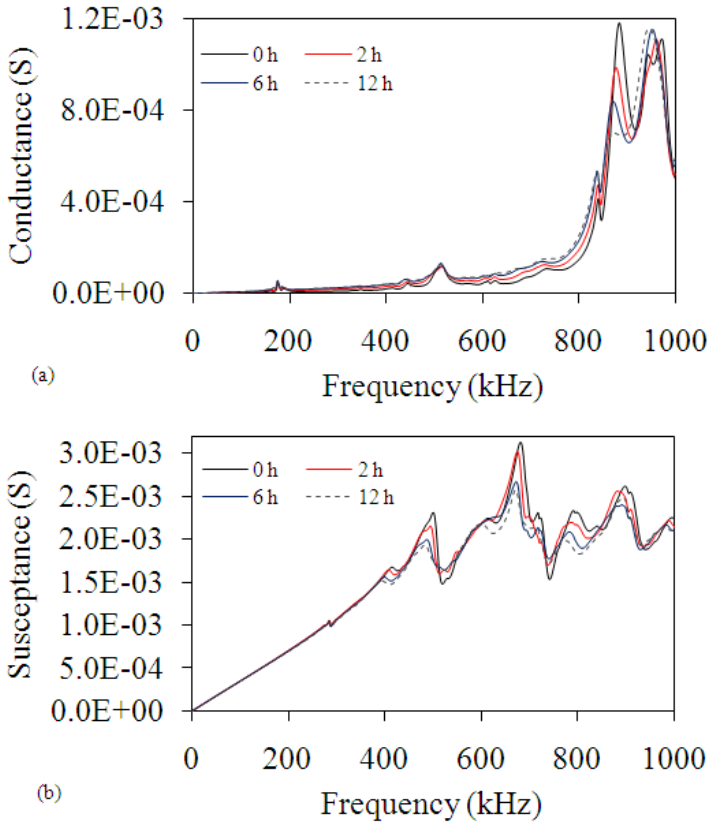

Figure 3.12: Test 2. Long implant: conductance (a) and susceptance (b) as a function of frequency

A close up view of figures 3.11a and 3.12a is presented in figure 3.13a and 3.13b for the short and the long implant respectively. Observing such a figures, the damping does not influence the response over the time, whereas the shift over lower frequencies is appreciable.

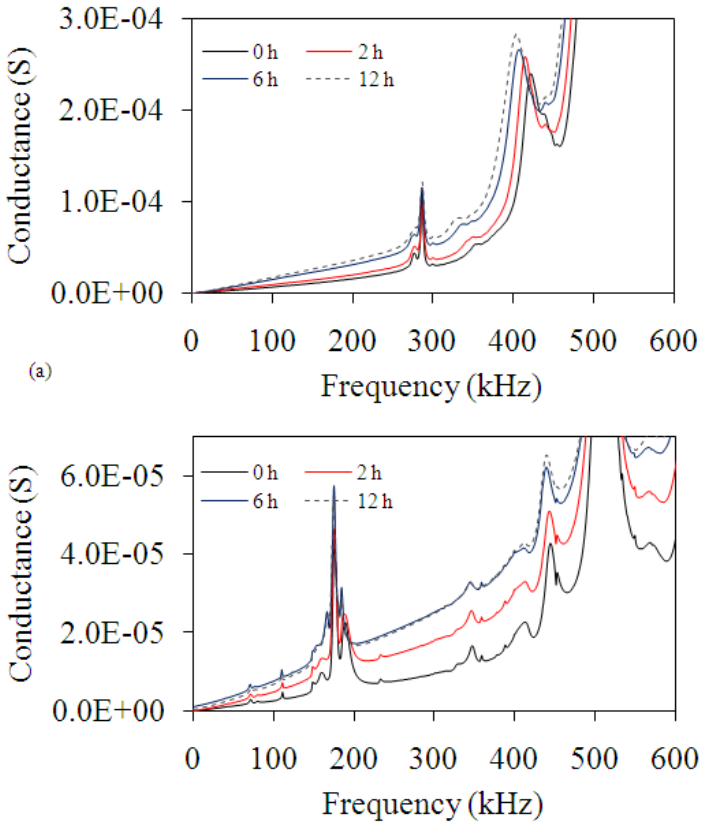

Figure 3.13: Test 2. Close up view at lower frequencies for short (a) and long (b) implant as a function of frequency

Figure 3.14 show the peak frequencies as a function of time for the long implant, whereas figure 3.15 for the short implant. When compared to the dense foam, the frequency shift is slighter more severe. This is due to the fact that the presence of larger voids accelerated the degradation process. It can be argued that the mass does not influence the sfhit to the lower frequencies, in fact, such behavior agree with what was observed.

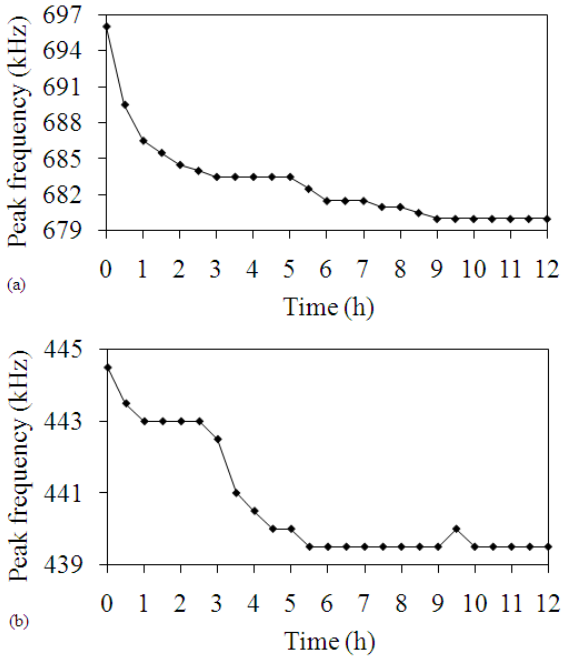

Figure 3.14: Test 2. Peak frequencies as a function of time for the short implant

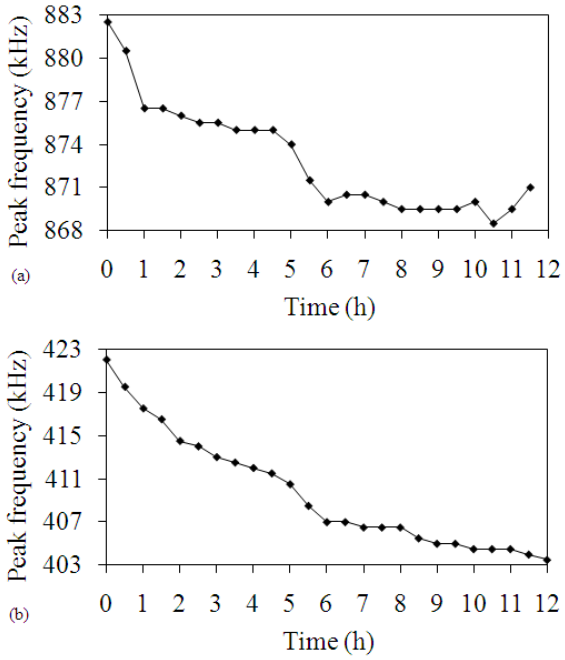

Figure 3.15: Test 2. Peak frequencies as a function of time for the long implant

Figures 3.16a and 3.16b show the RMSD and the RMS as a function of the monitoring time for both implants. The outcome from the analysis of the RMS is somehow inconclusive as the largest variation from the baseline is in the order of 8%.

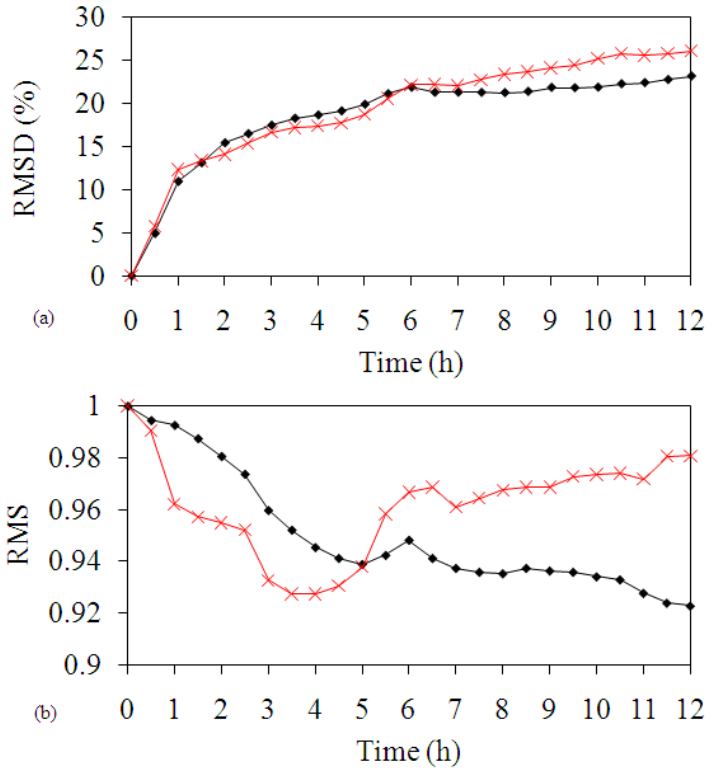

Figure 3.16: Test 2. RMSD and RMS as a function of time for short (dots) and long (x) implant

With the respect of the slope the figure 3.17 shows as the variation of the conductance signatures is lower compared to the hard polyurethane. In fact the max negative slope is 4×10^{-5} for the short implant.

For completeness the figure 3.18a shows the conductance at 688 kHz as a function of time for the short implant, whereas 3.18b represents the response at 880 kHz for the long implant. Such a frequencies reflect the max (negative) slope. Similarly to the hard polyurethane, the linear trend is observed.

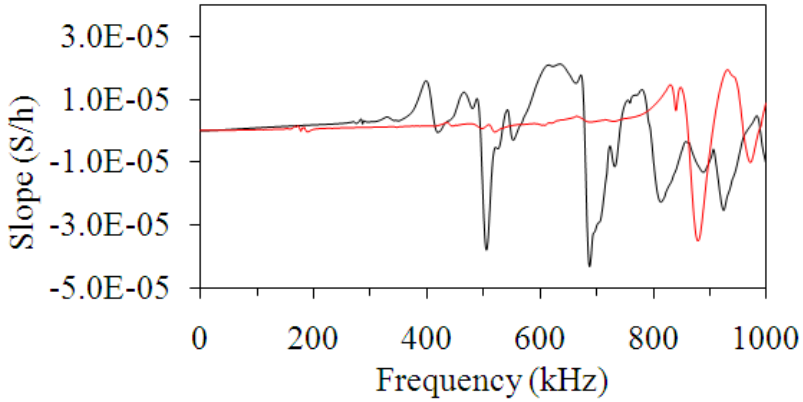

Figure 3.17: Test 2. Slope as function of frequency for short (black line) and long (red line) implant.

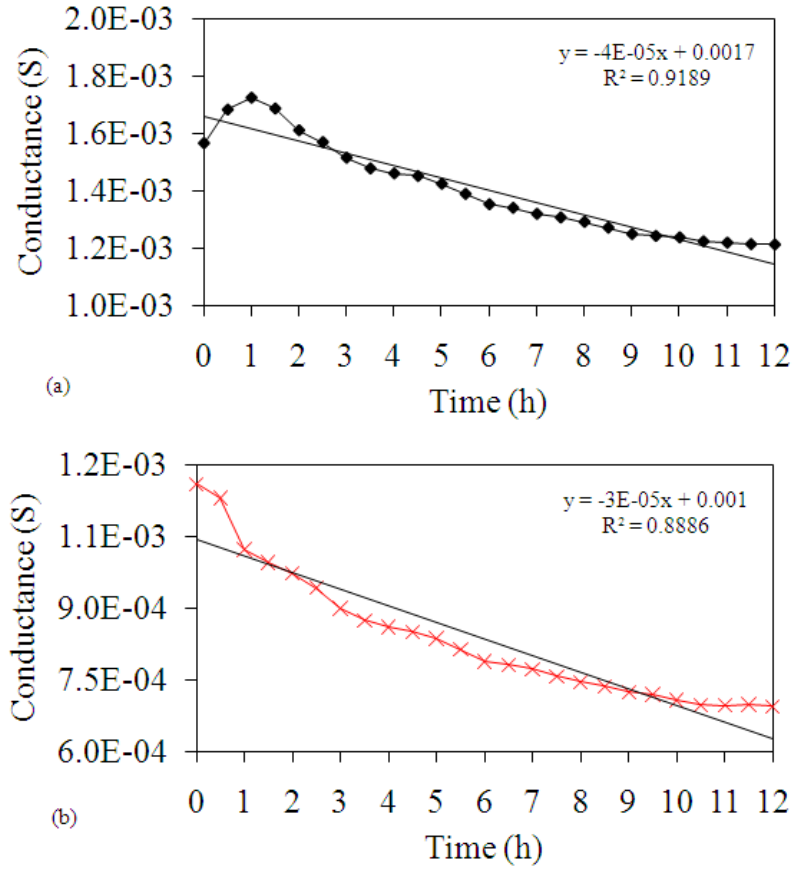

Figure 3.18: Test 2. Conductance at 688 kHz for the short implant (a) and at 880 kHz for the long implant (b) as a function of time

3.3 Test 3. Joint Compound

The figure 3.19a and 3.19b shows the conductance as a function of frequency associated to the PZT number 3 (long implant) at different monitoring time, namely, 0-12h and 1-9 days. A structural peak at 700 kHz is evident. Furthermore increasing the time leads to a narrower peak. A close-up view of the peaks visible at 200-300 kHz and 650-800 kHz range is presented in figure 3.20 and 3.21 respectively.

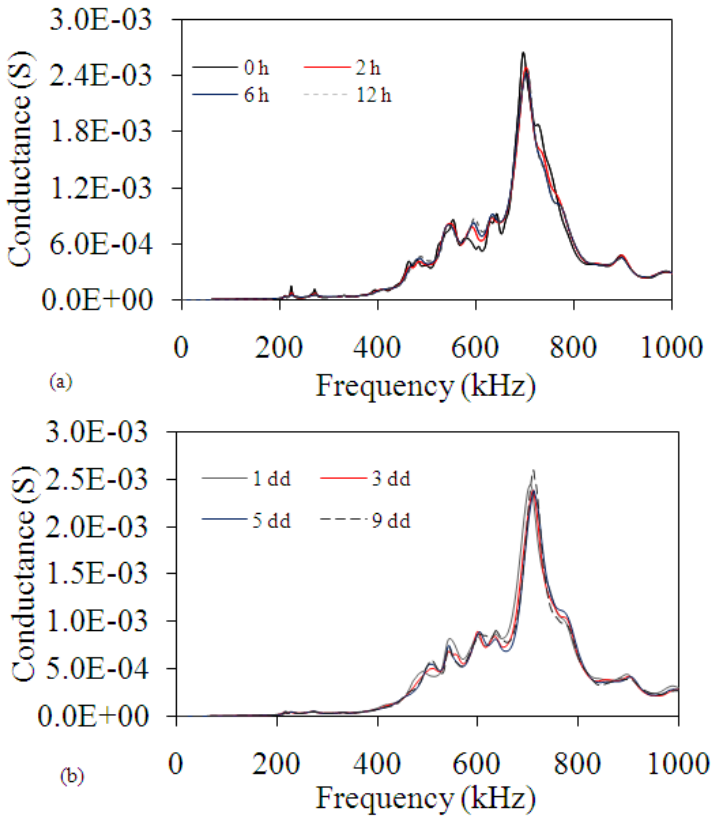

Figure 3.19: Test 3. Conductance as a function of frequency for PZT number 3 (long implant)

The low-frequency peaks denote a gradual shift towards higher frequencies and a monotonic decrease in amplitude. On the contrary the values of the conductance outside the peak cones increase during the first twelve hours (3.20a), but, observing figure 3.20b the conductance is slighter low; in addition, the peak at 210 kHz increase its amplitude

and a shift towards higher frequencies is more evident.

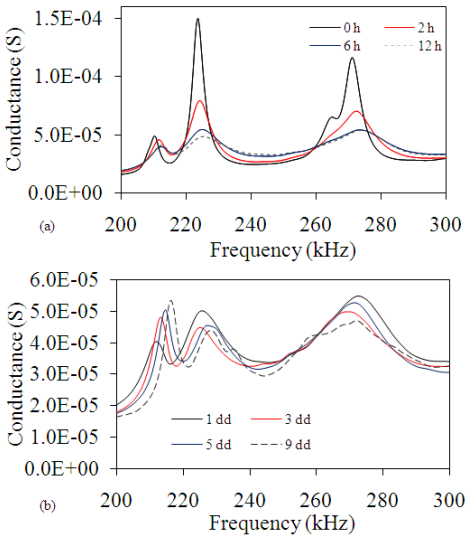

Figure 3.20: Test 3. Close up view of the conductance amog 200 kHz and 300 kHz for PZT number 3 (long implant)

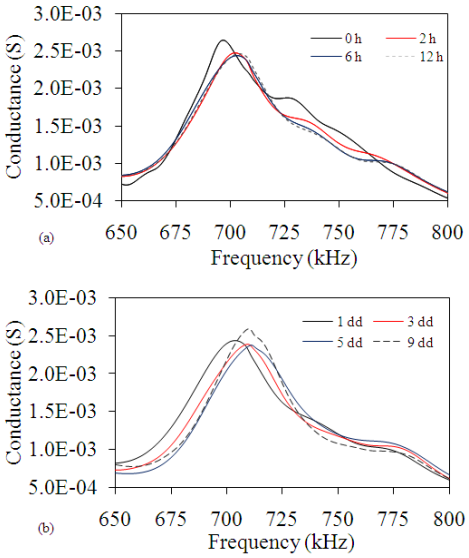

Figure 3.21: Test 3. Close up view of the conductance amog 650 kHz and 800 kHz for PZT number 3 (long implant)

The conductance signature associated with one short implant is presented in figure 3.22. Both the frequency and the amplitude of the conductance peak do not seem change significantly during the monitor-

ing time. Not shown here, the response of the second short implant was similar. This result confirms that the response of the electromechanical impedance of the PZT might be influenced by the implant length.

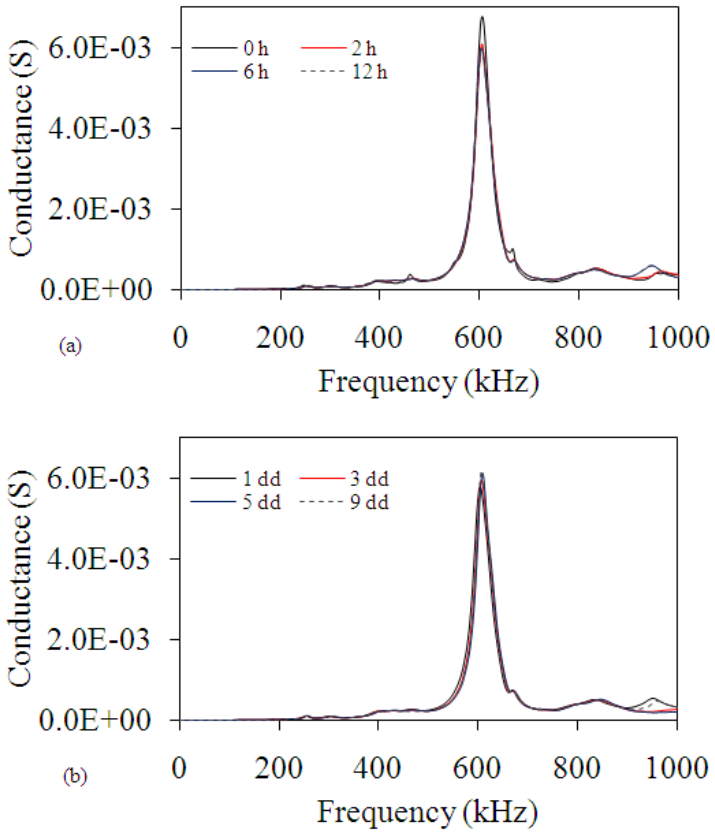

Figure 3.22: Test 3. Conductance as a function of frequency for PZT number 2 (short implant)

Figure 3.23 and 3.24 show the resonance peak frequencies as a function of monitoring time for all the implants. In detail figures 3.23a-d refer to PZT number 1 and figures 3.23e-f refer to PZT number 3, figure 3.24a-b is associated to the implant 2 and figure 3.24c-d is associated with the implant 4.

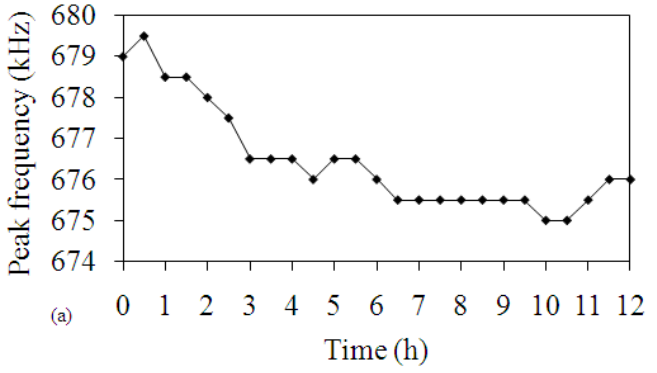
Peak frequency (kHz)
680
679
678
677
676
675
674
0 1 2 3 4 5 6 7 8 9 10 11 12
(a)
Time (h)

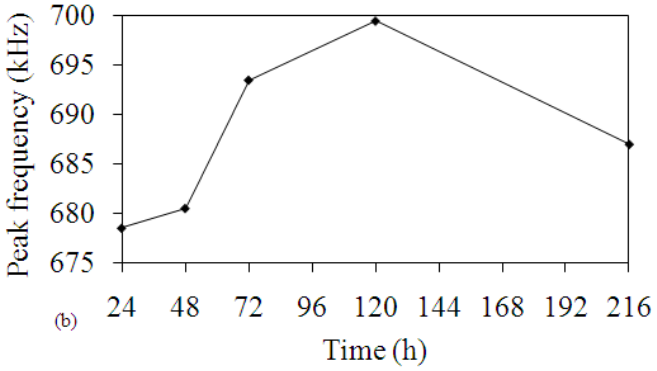
Peak frequency (kHz)
700
695
690
685
680
675
24 48 72 96 120 144 168 192 216
(b)
Time (h)

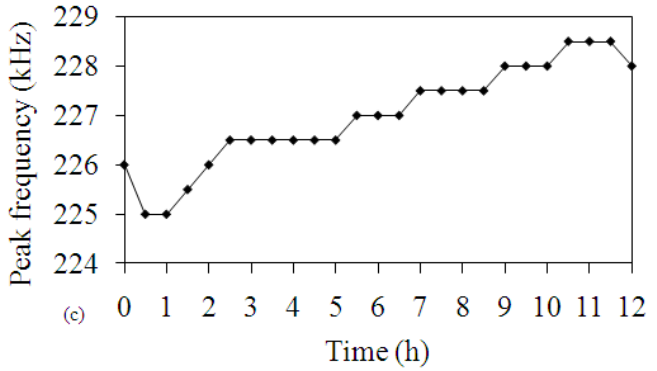
Peak frequency (kHz)
229
228
227
226
225
224
0 1 2 3 4 5 6 7 8 9 10 11 12
(c)
Time (h)

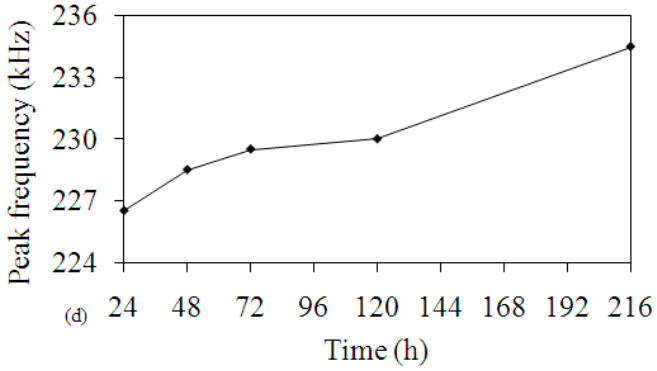
Peak frequency (kHz)
236
233
230
227
224
24 48 72 96 120 144 168 192 216
(d)
Time (h)

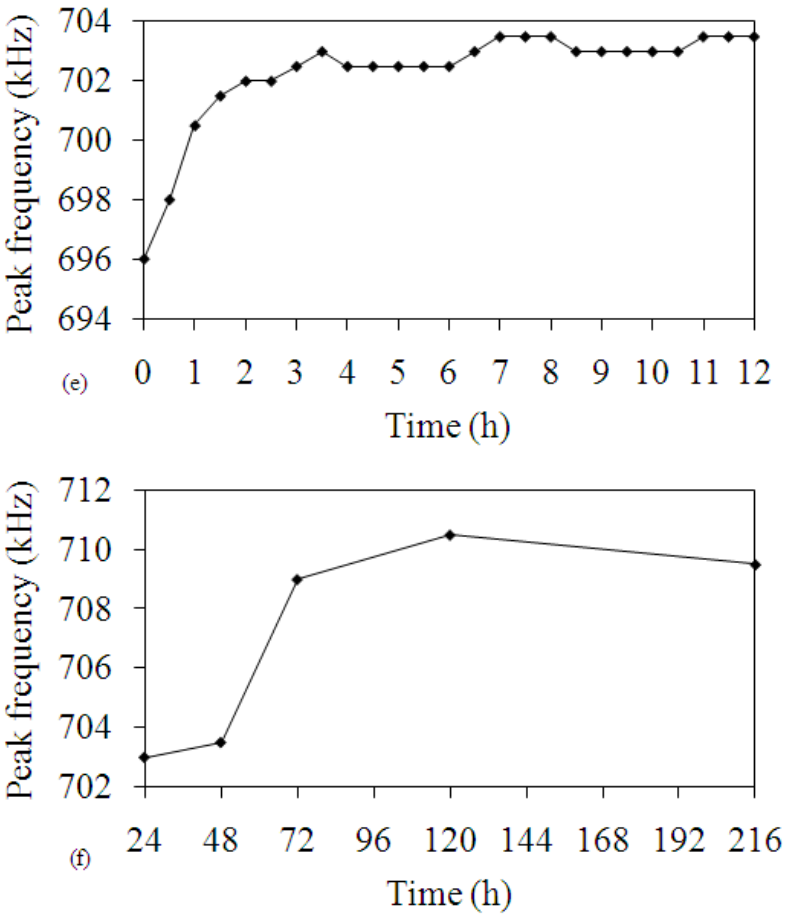

Figure 3.23: Test 3. Peak frequency as a function of time for PZT number 1 (a-d) and PZT number 3 (e-f)

Apart from few exceptions the frequency of the peaks shifts towards higher values as the joint compound sets into the alveoli. This response is opposite to what observed during the degradation process. As the compound sets, the stiffness of the system increases which cause an overall increase of the structural peak frequencies.

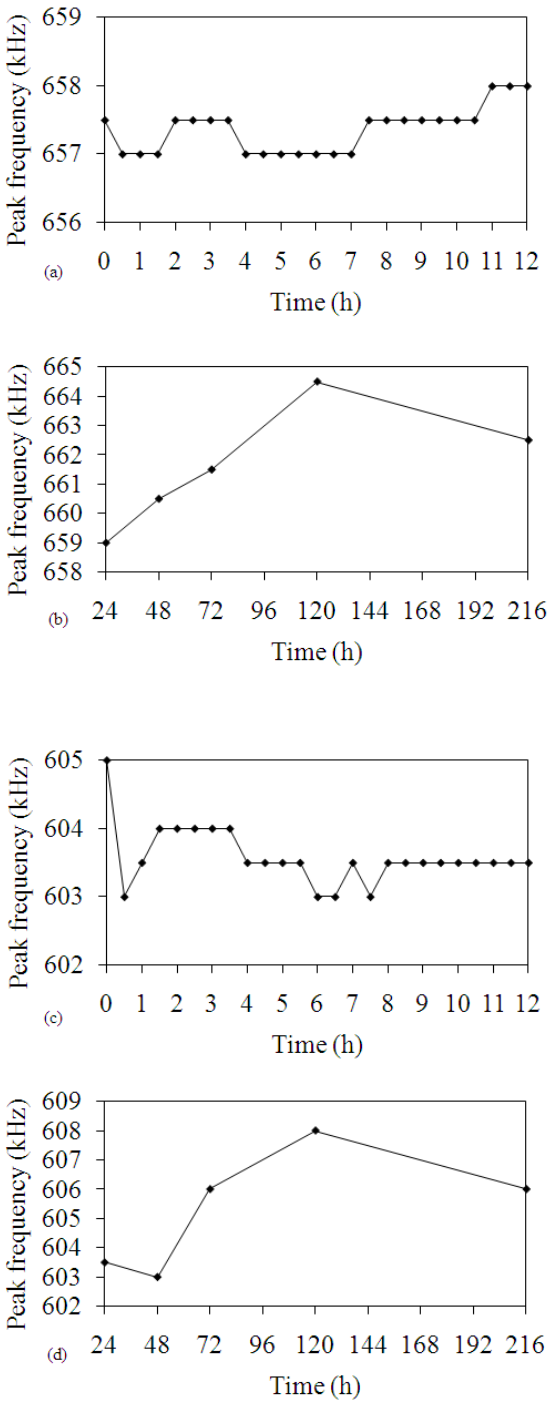

Figure 3.24: Test 3. Peak frequency as a function of time for PZT number 2 (a-b) and PZT number 4 (c-d)

Overall the trend is opposite to what observed during the degrada-

tion process. The frequency of the peak increased with time, i.e. with the increase of the stability of the implant inserted in the fresh compound. Finally, the peak shift trend is opposite to the peak shift trend observed for the polyurethane samples. This result is expected as, in Test 3, the consolidation process was monitored. It seems from the figure 3.23 that up to 120 hours the resonance peak shifts to higher frequencies, then, a decrease is observed. This shift was unexpected, nevertheless the peak increases its magnitude, thus a decrease of damping is observed. On other hands, the shift to lower frequencies is not observed for the lower peaks.

The value of the conductance slopes as a function of the excitation frequency is presented in figure 3.25 for all implants.

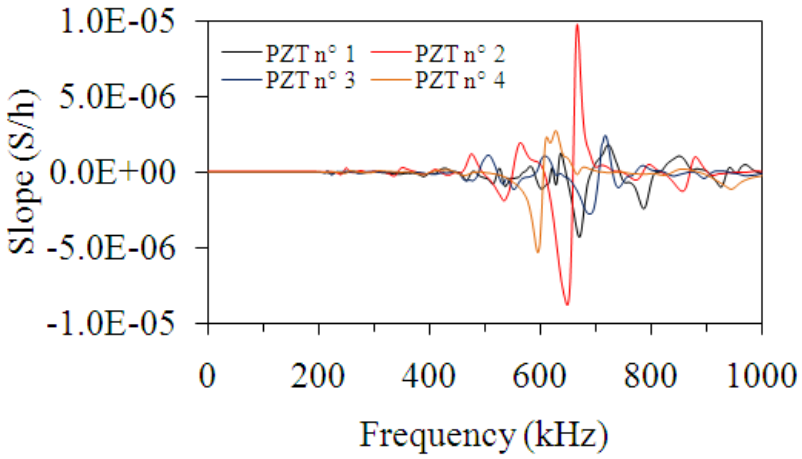

Figure 3.25: Test 3. Slope as function of frequency for all the implants

Although the overall shape of all curves is quite similar, the values of the peak and valleys is different as well as the frequencies at which they occur. It must be remarked that the highest positive slope associated with each implant is one or two order of magnitude smaller than those found in Tests 1 and 2.

Finally with the respect to RMSD and RMS, the figure 3.26 and 3.27 show such as signatures. The increase of RMSD is observed, since the resonance peaks encounter damping during the monitoring time at least

until 120 hours. Then, the peaks were observed more sharp and higher, thus, the RMSD decrease, as was expected. However, the RMSD, comparing to the degradation process, seems to be a good tool to evaluate how the conductance signatures vary over the time.

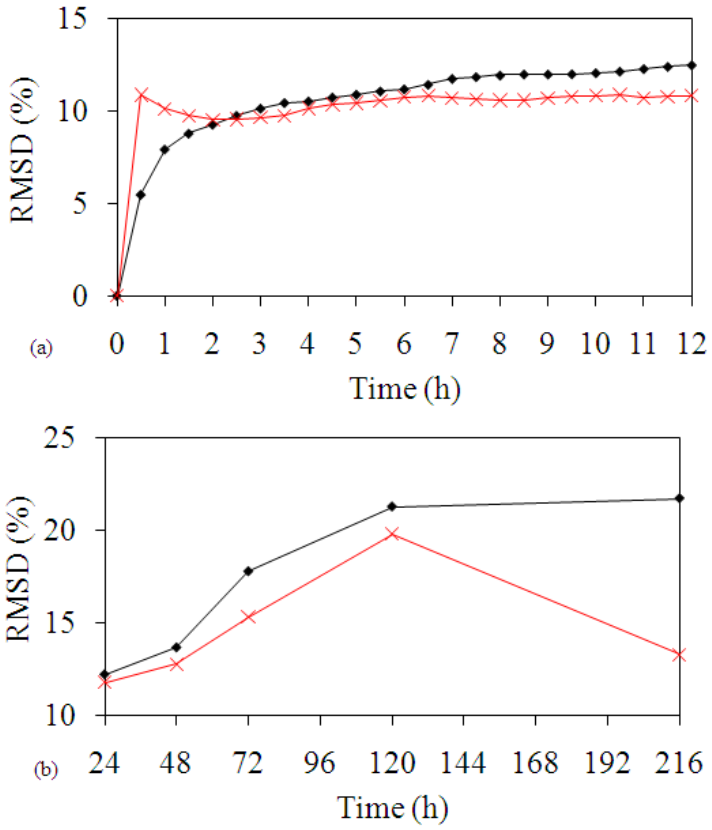

Figure 3.26: Test 3. RMSD (%) as a function of time for PZT number 3 (x red) and PZT number 2 (dots)

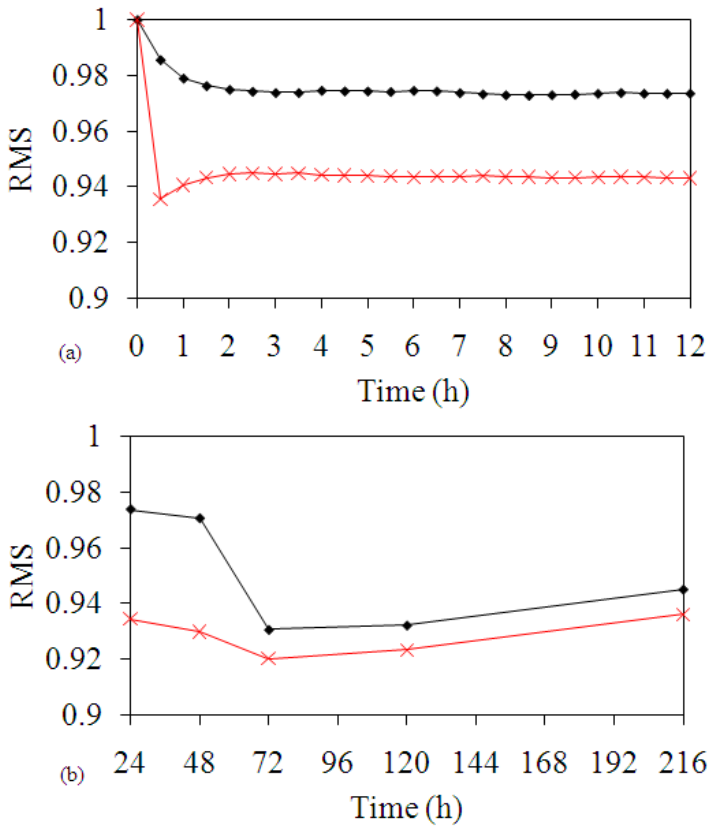

Figure 3.27: Test 3. RMS (normalized to the initial value) as a function of time for PZT number 3 (x red) and PZT number 2 (dots)

3.4 Mechanical test results

The mechanical tests were conducted with the aim to compare the results with those obtained by electro-mechanical impedance method. The figure 3.28 shows the stress-strain plot at different degradation time, namely, 0h,2h and 12h; it should be noted that the right axis refers to the 12h signature. The loss of mechanical properties is evident.

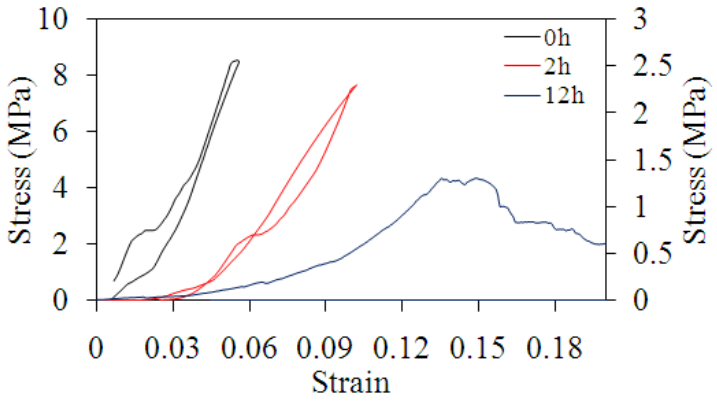

Figure 3.28: Compression test. Stress-strain plot for different degradation time

Chapter 4

Discussion

Nowadays, assessment of implant stability by means of non destructive evaluation such as resonance frequency analysis and periotest is still under investigation although their use is spread [76]. Indeed, the clinicians relies on their experience rather than such instruments. On other hands, if their reliability is enhanced, certainly such techniques might be the best tools to evaluate implant stability.

Different implant geometries, bone like materials and trasducers were used in order to prove the effectiveness and reliability of the electromechanical impedance method. The dynamical interaction over the time among the structure and the PZT was monitored. Therefore, features as mass, stiffness and damping have to be taken in account in order to assess the frequency response of the structure.

Regarding the decomposition process the conductance underwent to progressive increase as the nitric acid effect was stronger. It can be argued that the values of the conductance within these ranges are related to the polyurethane stiffness. As proved by *Brosh et al* [111], the stiffness of the bone-implant interface during healing time increases due to anchorage of the bone to the implant surface. Therefore it can be inferred that the EMI method will be indirectly able to assess the stiffness of the bone-implant system by monitoring the admittance characteris-

tics of a PZT attached to the implant. Moreover, it is believed that the shift to the lower frequencies is associated with the decrease of the polyurethane stiffness while the shifts towards higher frequencies (figure 3.6a,3.7b) observed after several hours is probably due to mass reduction of the specimen.

The following figure 4.1 shows the peak frequency associated to the different foam densities and implant geometry.

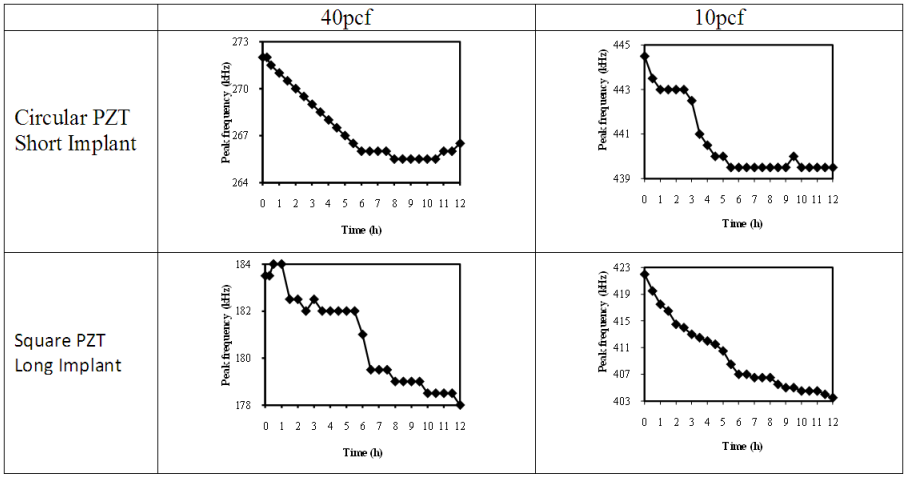

Figure 4.1: Comparison of peak frequency for decomposition test

The shift to lower frequencies is evident for all the conditions, therefore, it can be concluded that the EMI response is robust enough to different boundary conditions. Moreover, figure 4.2 shows the peak frequencies with the same PZT. Similar results are achieved.

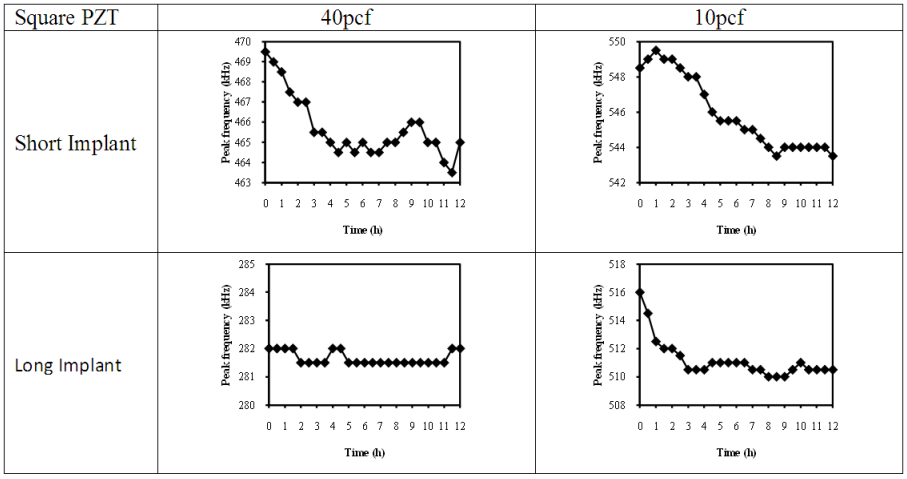

Figure 4.2: Comparison of peak frequency for decomposition test

With the respect to the RMSD the following figures 4.3,4.4 show a comparison of RMSD.

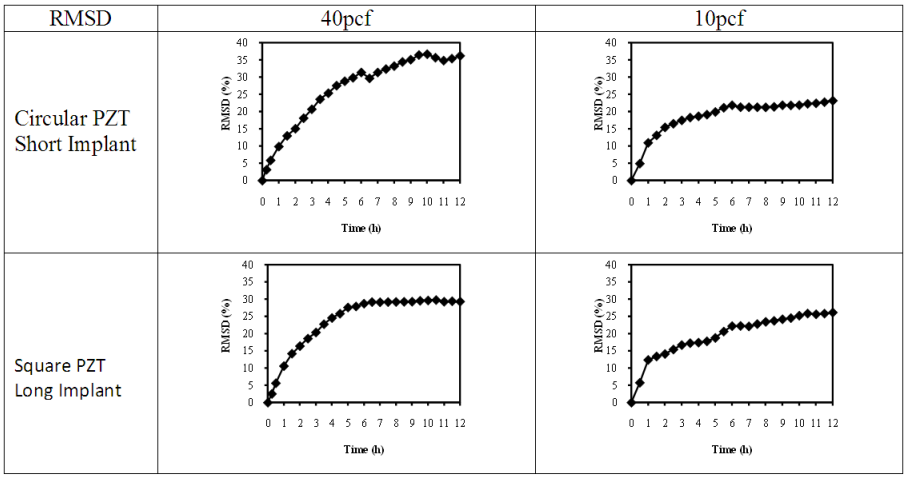

Figure 4.3: Comparison of RMSD for decomposition test

Even such feature shows prominent results in terms of robustness of the electro-mechanical impedance method. In fact, the trend of the RMSD is similar for all the figures, even if, quantify this variation seems to be somehow heavy, for instance, the 80% for the short implant associated to the 10pcf foam was unexpected.

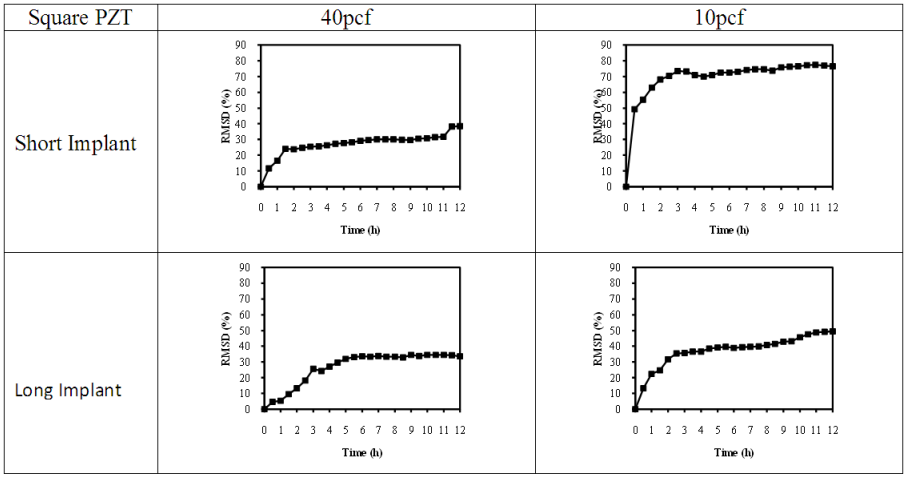

Figure 4.4: Comparison of RMSD for decomposition test

From the mechanical tests, the Young modulus was calculated and plotted in the figure 4.5 overlapped to the RMSD signature. The trend is particularly similar to the RMSD, moreover, as is possible notice on the right axis, the young modulus loss reaches 92 % at 12 hours of degradation.

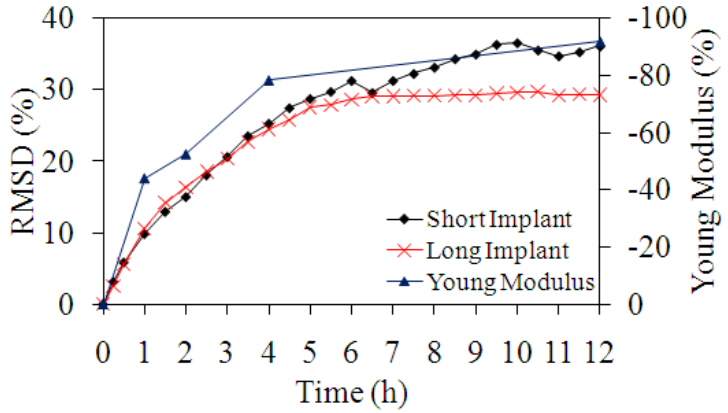

Figure 4.5: Compression test. Young modulus loss as a function of time, overlapped to the RMSD signature

Considering the healing test the results confirm what it has been said for the denser foam and demonstrate the effectiveness of the EMI to monitor the evolution of the material stiffness as well as the stiffness

of the material-implant interface. In addition, the results agree with the findings of *Soh and Bhalla* [22] and *Shin et al* [110] where the curing age of concrete was monitored by means of EMI. They found similar results in terms of stiffness, in fact, a shift to higher frequency is observed as the curing time increase; nevertheless with the respect to the damping the results were somehow discordant.

Overall the following conclusion are arisen:

i the EMI method can be a potential method to evaluate implant stability;

ii statistical features such as RMSD can lead to a new way to assess bone condition around a dental implant;

iii like the others modal analysis, the EMI method may be influenced by implant geometry;

iv the sensitivity to assess the bone changes during the osseointegration is not predictable with this experimental study.

Chapter 5

Conclusions

In this paper a feasibility study about the use of the electromechanical impedance method to assess the stability of dental implants is presented. Dental prostheses of two different geometries were tested by entrenching them in three different materials, namely high- and low-density polyurethane and a joint compound. Inverse bone healing was simulated by exposing the polyurethane samples to a solution of nitric acid and allowing the degradation process for several hours. The process was indirectly monitored by measuring the admittance signature of piezoelectric transducers bonded onto the head of each implant. The direct bone healing process was instead monitored by surrounding the implants with a thin layer of fresh joint compound and embedding them in a coupon made of compound previously set.

The sensitivity of the conductance with respect to the structural impedance of the PZT-implant-specimen system was quantified using the conventional statistical feature of RMSD,the features associated with the RMS of the admittance signatures, and the conductance slope, i.e. the gradient of the conductance with respect to time.

Overall, the experiments showed a shift of the frequency peaks toward the lower frequencies when degradation was observed and toward higher frequencies when setting was monitored. As the frequency reso-

lution of the equipment was 500 Hz, it is possible that some impedance peaks were missed. The use of both the RMSD and the RMS applied to the conductance signatures show a significant variation of the electromechanical properties of the transducers with respect to the material properties. Between the two statistical indices, the RMSD showed more promising results. The quantitative variations observed among the various experiments and implants were attributed to the geometric properties of the implants.

The quantitative values of the RMSD were then compared to the stiffness and the Young modulus of high-density polyurethane exposed to the same solution of nitric acid. The correlation between the electromechanical results and the destructive test was demonstrated.

Although SAWBONE is universally recognized as a material that reproduces bone tissue well, joint compound does not. Therefore, it must be acknowledged that the amount of fresh compound around the screw might not have been thoroughly representative of the amount and quality of bone tissue that forms around real implants during the healing process. In addition, it is known that in general a perfect three-dimensional congruity will not exist between a surgically prepared bone site and the surface of a dental implant. Micro-and macro-gaps are, in fact, initially filled with blood clots. Then, bone heals in the gap by a process called intramembranous bone formation [62].

Finally, the frequency interval used in the experiments might have suffered from inadequate resolution to resolve and quantify the frequency shifts of peaks in individual vibration modes.

Although aliasing might have been possible, it is believed that this study provided sufficient experimental evidence to encourage further study on the application of EMI for dental implant assessment.

Bibliography

[1] Boronat-López A., Peñarrocha-Diago M., Martínez-Cortissoz O., and Mínguez-Martínez I. Resonance frequency analysis after the placement of 133 dental implants. *Med Oral Patol Oral Cir Bucal*, 11:272–276, 2006.

[2] Deporter D. A, Friedland B., and Watson P. A. A clinical and radiological assessment of a porous-surfaced ti alloy dental implant system in dogs. *J. Dent. Res*, 65:1071–1077, 1986.

[3] Samiotis A. Clinical monitoring with resonance frequancy analysis (rfa) of astra implants a clinical study. *Int Poster J Dent Oral*, 5, 2003.

[4] Tabassum A, Meijer G.J, and Jansen J. A Wolke J. G. C. Influence of surgical technique and surface roughness on the primary stability of an implant in artificial bone with different cortical thickness: a laboratory study. *Clinical Oral Implants Research*, 21:213–220, 2009.

[5] Friberg B., Sennerby L., Meredith N., and Lekholm U. A comparison between cutting torque and resonance frequency measurements of maxillary implants. a 20-month clinical study. *Int J Oral Maxillofac Surg*, 28:297–303, 1999.

[6] Aparicio C. The use of the periotest value as the initial success criteria of an implant: 8-year report. *Int J Periodontics Restorative Dent*, 17:150–161, 1997.

[7] Aparicio C., Perales P., and Rangert B. Tilted implants as an alternative to maxillary sinus grafting: a clinical, radiologic, and periotest study. *Clin Implant Dent Relat Res*, 3:39–49, 2001.

[8] Bechtol C. Internai fixation with plates and screws. In *Metals and Engineering in bone and joint surgery*, 1959.

[9] Liang C., Sun F.P., and Rogers C.A. Coupled electro-mechanical analysis of adaptative material systems-determination of the actuator power consumption and system energy transfer. *Journal of Intelligence Material Systems and Structures*, 5:12, 1994.

[10] Misch C. *An implant is not a tooth: a comparison of periodontal index*, volume 1. Dental Implant Prosthetics, 2005.

[11] Po-Chun C, Niklaus P.L., and William V.G. Evaluation of functional dynamics during osseointegration and regeneration associated with oral implants. *Clinical Oral Implants Research*, 21:1–12, 2009.

[12] Johansson C.B., Han C.H., Wennerberg A., and Albrektsson T. A quantitative comparison of machined commercially pure titanium and titanium-aluminium-vanadium implants in rabbit bone. *Int J Oral Maxillofac. Implants*, 13:315–321, 1998.

[13] Cheng C.C. and Lin C.C. An impedance approach for determining optimal locations and shapes of multiple induced strain actuators. *Smart Materials and Structures*, 14:1120–1126, 2005.

[14] Ciang C.C., Lee J.R., and Bang H.J. Structural health monitoring for a wind turbine system: a review of damage detection methods. *Measurement Science and Technology*, 19:1–20, 2008.

[15] Misch C.E. Bone classification, training keys to implant success. *Dent Today*, 8:39–44, 1989.

[16] Misch C.E. Density of bone: effect on treatment plans, surgical approach, healing, and progressive boen loading. *Int J Oral Implantol*, 6:23–31, 1990.

[17] Misch C.E. The implant quality scale: a clinical assessment of the health–disease continuum. *Oral Health*, 88:15–20, 23–5; quiz 25–6, 1998.

[18] Misch CE. *Contemporary Implant Dentistry*, volume 3. 2008.

[19] Misch C.E. and Misch C.M. Generic terminology for endosseous implant prosthodontics. *J Prosthet Dent*, 68:809–812, 1992.

[20] Misch C.E., Wang H.L., and Palti A. The international congress of oral implantologists consensus congress on implant success. In *Pisa, Italy*, 2007.

[21] Misch C.E., Qu Z., Bidez M., and Misch C.E. Mechanical properties of trabecular bone in the human mandible: implications for dental implant treatment planning and surgical placement. *J Oral Maxillofac Surg*, 57:700–706, 1999.

[22] Soh C.K. and Bhalla S. Calibration of piezo-impedance transducers for strength prediction and damage assessment of concrete. *Smart Materials and Structures*, 14:671–684, 2005.

[23] Tisdel C.L., Goldberg V.M., Parr J.A., Bensusan J.S., Staikoff L.S., and Stevenson S. The influence of a hydroxyapatite and tricalcium-phosphate coating on bone growth into titanium fiber-metal implants. *J Bone Joint Surg Am*, 76:159–171, 1994.

[24] Ten Bruggenkate C.M., van der Kwast V.A., and Oosterbeek H.S. Success criteria in oral implantology. a review of the literature. *Int J Oral Implantol*, 7:45–51, 1990.

[25] Farrar C.R. and Sohn H. Pattern recognition for structural healt monitoring. In *Workshop on Mitigation of Earthquake Disaster by Advanced Technologies (Las Vegas, NV, USA)*, 2000.

[26] Andrade J. D and Hlady V. *Protein adsorption and materials biocompatibility: a tutorial review and suggested hypotheses*. 1987.

[27] Buser D., Schenk R.K., Steinemann S., Fiorellini J.P., Fox C.H., and Stich H. Influence of surface characteristics on bone integration of titanium implants. a histomorphometric study in miniature pigs. *Journal of Biomedical Materials Research*, 25:889–902, 1991.

[28] Steenberghe D. and Jacobs R. *Radiographic planning and assessment of endosseosus oral implants*, volume 1. 1998.

[29] Tinsley D, Watson CJ, and Ogden AR. A survey of uk centres on implant failures. *J Oral Rehabil*, 26:14–18, 1999.

[30] Holmes D.C. and Loftus J.T. Influence of bone quality on stress disribution for endosseous implants. *Journal of Oral Implantology*, 23:104–111, 1997.

[31] Cochran D.L., Schenk R.K., Higginbotto F.L., Lussi A., and Buser D. Bone response to unloaded and loaded titanium implants with a sandblasted and acid etched surface. a histometric study in the canine mandible. *J Biomed Mater Res*, 40:1–11, 1998.

[32] Sullivan D.Y., Sherwood R.L., Collins T.A., and Krogh P.H. The reverse-torque test: a clinical report. *J Oral Maxillofac Implants*, 11:179–185, 1996.

[33] Nkenke E., Hahn M., Weinzierl K., Troger M., Neukam F.W., and Engelke K. Implant stability and histomorphometry: a correlation study in human cadavers using stepped cylinder implants. *Clinical Oral Implants Research*, 14:601–609, 2003.

[34] Richter E.J. Basic biomechanics of dental implants in prosthetic dentistry. *Journal of Prosthetic Dentistry*, 61:602–609, 1989.

[35] Richter E.J. In vivo horizontal bending moments on implants. *International Journal of Oral and Maxillofacial Implants*, 13:232–244, 1998.

[36] Lautenschlager E.P. and Monaghan P. Titanium and titanium alloys as dental materials (review). *Int Dent J*, 43:245–253, 1993.

[37] Colaizzi F.A., Javid N.S., Micheal C.G., and Gibbs C.J. Biting force, emg, and jaw movements in denture wearers. *J Dent Res*, 13:63–329, 1984.

[38] Dahl G. Dental implants and superplants. *Rassegna Trimestrale Odont*, 4:25–36, 1956.

[39] Dahl G. Some aspects of the use of intramucosal inserts. *J Oral Implant Transplant Surg*, 12:61–65, 1966.

[40] Jividen G. and Misch C.E. Reverse torque testing and early loading failures: help or hindrance? *J Oral Implantology*, 26:82–90, 2000.

[41] Park G., Sohn H., Farrar C.R., and Inman D.J.

[42] Park G., Cudney H.H., and Inmann D.J. Feasibility of using impedance-based damage assessment for pipeline structures. *Earthquake Eng Struct Dyn*, 30:1463–1474, 2001.

[43] Thompson G. and Puleo D.A. Ti-6al-4v ion solution inhibition of osteogenic cell phenotype as a function of differentiation time-course in vitro. *Biomaterials*, 17:1949–1954, 1996.

[44] Watzek G. *Implants in qualitatively compromised bone*, volume 1. 2004.

[45] Carlsson G.E. Functional response. *In Branemark PI and Zarb G Tissue Integrated Prostheses.Chicago: Quintessence Publ. Co.*, pages 155–163, 1985.

[46] Carlsson G.E. and Haraldsson T. Bite force and chewing efficiency. *Front Oral Physiol*, 6:265–292, 1974.

[47] Salvi G.E. and Lang N.P. Diagnostic parameters for monitoring peri-implant conditions. *Int J Oral Maxillofac Implants*, 19 Suppl:116–127, 2004.

[48] Cameron H., Pilliar R. M., and Macnab I. The effect of movement on the bonding of porous metal to bone. *J. Biomed. Mater. Res.*, 7:301–311, 1973.

[49] Graf H. Occlusal force during function. *In: Rowe N.H. Occlusion: research on form and function. Ann Arbor: University of Michigan*, pages 90–111, 1975.

[50] Plenk H.Jr and Zitter H. *Endosseous implants: scientific and clinical aspects*, volume 1. 1996.

[51] Friberg H.M. Presence of microscopic cracks in vivo in bone. *Bulletin of Henry ford Hospital*, 8:25–35, 1960.

[52] Miyamoto I., Tsuboi Y., Wada E., Suwa H., and Iizuka T. Influence of cortical bone thickness and implant length on implant stability at the time of surgeryclinical, prospective, biomechanical, and imaging study. *Bone*, 37:776–780, 2005.

[53] Naert I., van Steenberghe D., and Worthington P. *Osseointegration in Oral Rehabilitation*, volume 1. 1993.

[54] Lincks J., Boyan B., Cochran D.L., Liu Y., Blanchard C., Dean D.D., and Schwartz Z. Mg53 cells discriminate between surface roughness and material composition. *J Dent Res*, 1998.

[55] Olivé J. and Aparicio C. Periotest method as a measure of osseointegrated oral implant stability. *Int J Oral Maxillofac Implants*, 5:390–400, 1990.

[56] Roze J., Babu S., Saffarzadeh A., Gayet-Delacroix M., Hoornaert A., and Layrolle P. Correlating implant stability to bone structure. *Clinical Oral Implants Research*, 20:1140–1145, 2009.

[57] Sirohi J. and Chopra I. Fundamental understanding of piezoelectric strain sensors. *Journal Intelligent Material Systems and Structures*, 11:243–257, 2000.

[58] Teerlinck J., Quirynen M., Darius P., and van Steenberghe D. Periotest: an objective clinical diagnosis of bone apposition toward implants. *Int J Oral Maxillofac Implants*, 6:55–61, 1991.

[59] Tricio J., Laohapand P., van Steenberghe D., Quirynen M., and Naert I. Mechanical state assessment of the implant-bone continuum: a better understanding of the periotest method. *Int J Oral Maxillofac Implants*, 10:43–49, 1995a.

[60] Tricio J., van Steenberghe D., Rosenberg D., and Duchateau L. Implant stability related to insertion torque force and bone density: An in vitro study. *J Prosthet Dent*, 74:608–612, 1995b.

[61] Brunski J.B. Biomechanical factors affecting the bone-dental implant interface. *Clin Mater*, 10:153–201, 1992.

[62] Brunski J.B. In-vivo bone response to biomechanical loading at the bone/dental-implant interface. *Adv Dent Res*, 13:99–119, 1992.

[63] Brunski J.B. and Hipp J.A. In vivo forces on endosteal implants: a measurement system and biomechanical considerations. *Journal of Prosthetic Dentistry*, 51:82–90, 1984.

[64] Bobyn J.D., Mortimer E.S., Glassman A.H., Engh C.A., Miller J.E., and Brooks C.E. Producing and avioding stress shielding: laboratory and clinical observations of noncemented total hip arthroplasty. *Clinical Orthopaedics and Related Research*, pages 79–96, 1992.

[65] Devies J.E. Understanding peri-implant endosseosus healing. *Transfer of Advances in Sciences into Dental Education*, 67:932–949, 2003.

[66] Ellingsen J.E. Surface configurations of dental implant. *Periodontology 2000*, 17:36–46, 1998.

[67] Hermann J.S., Cochran D.L., Nummikoski P.V., and Buser D. Crestal bone changes around titanium implants: a radiographic evaluation of unloaded nonsubmerged and submerged implants in the canine mandible. *J Periodontal*, 68:117–1130, 1997.

[68] Ayres J.W, Lalande F, Chaudhry Z, and Rogers C.A. Qualitative impedance-based health monitoring of civil infrastructures. *Smart Materials Structures*, 7:599–605, 1998.

[69] Bender J.W., Friedman H.I., Giurgiutiu V., Watson C., Fitzmaurice M., and Yost M.L. The use of biomedical sensors to monitor capsule formation around soft tissue implants. *Ann Plast Surg*, 56:72–77, 2006.

[70] Chai J.Y., Yamada J., and Pang I.C. In vitro consistency of the periotest instrument. *J Prosthodont*, 2:9–12, 1993.

[71] Hayashi K., Inadome T., Tsumura H., Nakashima Y., and Sugioka Y. Effect of surface roughness of hydroxyapatite-coated titanium on the bone-implant interface shear strength. *Biomaterials*, 15:1338–1345, 1994.

[72] Cristofolini L., Varini E., Pelgreffi I., Cappello A., and Toni A. Device to measure intra-operatively the primary stability of cementless hip stems. *Medical Engineering and Physics*, 28:475–482, 2006.

[73] Walker L., Morris H.F., and Ochi S. Periotest values of dental implants in the first 2 years after second-stage surgery: Dicrg interim report no. 8. dental implant clinical research group. *Implant Dent*, 6:207–212, 1997.

[74] Pastrav L.C., Jaecques S.V., Jonkers I., Perre G.V., and Mulier M.

[75] Hench LL and Wilson J. *An introduction to bioceramics-Advanced Series in Ceramics*, volume 1. 1993.

[76] Atsumi M., Park S.H., and Wang H.L. Methods used to assess implant stability: current status. *Int J Oral Maxillofac Implants*, 22:743–754, 2007.

[77] Esposito M., Hirsch J.M., Lekholm U., and Thomsen P. Biological factors contributing to failures of osseointegrated oral implants. (i). success criteria and epidemiology. *European Journal of Oral Science*, 106:527–551, 1998a.

[78] Esposito M., Hirsch J.M., Lekholm U., and Thomsen P. Biological factors contributing to failures of osseointegrated oral implants. (ii). etiopathogenesis. *European Journal of Oral Science*, 106:721–764, 1998b.

[79] Ogiso M., Yamashita M., and Matsumoto T. The process of physical weakening and dissolution of the ha-coated implant in bone and soft tissue. *J Dent Res*, 77:1426–1434, 1998.

[80] Viceconti M., Brusi G., Pancanti A., and Cristofolini L. Primary stability of an anatomical cementless hip stem: A statistical analysis. *J Biomech*, 39:1169–1179, 2006.

[81] Huwiler M.A., Pjetursson B.E., Bosshardt D.D., Salvi G.E., and Lang N.P. Resonance frequency analysis in relation to jawbone characteristics and during early healing of implant installation. *Clin Oral Implants Res*, 18:275–280, 2007.

[82] Zablotsky M.H. Hydroxyapatite coatings in implant dentistry (review). *Implant Dent*, 1:253–257, 1992.

[83] Meredith N. A review of nondestructive test methods and their application to measure the stability and osseointegration of bone anchored endosseous implants. *Crit Rev Biomed Eng*, 26:275–291, 1998a.

[84] Meredith N. Assessment of implant stability as a prognostic determinant. *Int J Prosthodont*, 11:491–501, 1998b.

[85] Meredith N., Alleyne D., and Cawley P. Quantitative determination of the stability of the implant-tissue interface using resonance frequency analysis. *Clin Oral Implants Res*, 7:261–267, 1996.

[86] Meredith N., Shagaldi F., Alleyne D., Sennerby L., and Cawley P. The application of resonance frequency measurements to study the stability of titanium implants during healing in the rabbit tibia. *Clin Oral Implants Res*, 8:234–243, 1997.

[87] Ducheyne P., De Meester P., Aernoult E., Martens M., and Mulier C. Influence of a functional dynamic loading on bone ingrowth into surface pores of orthopaedic implants. *J. Bio-From the experimental literature it appears that it is not med. Mater. Res.*, 1:811–838, 1977.

[88] Thiel P.A and Madey T.E. The interaction of water with solid surfaces: fundamental aspects. *Surface Sci Rep*, 97:211–385, 1987.

[89] Branemark P.I. Intraosseuous anchorage of dental prosthesis. experimental studies. *Scand. J. Plast. Reconstr. Surg.*, 3:81–100, 1969.

[90] Branemark P.I, Zarb G. A, and Albrektsson T. Tissue integrated prostheses: Osseointegration in clinical dentistry. *Chicago: Quintessence Publ. Co.*, 1985.

[91] Glantz P.O., Rangert B., Svensson A., Stafford G.D., Arnvidarson B., and Randow K. et al. On clinical loading of osseointegrated implants. a methodological and clinical study. *Clinical Oral Implants Research*, 4:99–105, 1993.

[92] Ostman P.O., Hellman M., Wendelhag I., and Sennerby L. Resonance frequency analysis measurements of implants at placement surgery. *Int J Prosthodont*, 19:77–83, 2006.

[93] Binon P.P. Implants and components: entering the new millennium. *Int J Oral Maxillofac Implants*, 15:76–94, 2000.

[94] Haas R., Bernhart T., Dörtbudak O., and Mailath G. Experimental study of the damping behaviour of imz implants. *J Oral Rehabil*, 26:19–24, 1999.

[95] Nedir R., Bischof M., Szmukler-Moncler S., Bernard J.P, and Samson J. Predicting osseointegration by means of implant primary stability. *Clin Oral Implants Res*, 15:520–528, 2004.

[96] Craig R.G. Restorative dental materials. *St Louis, Mo: C.V.Mosby*, 6:60–61, 1980.

[97] Barewal R.M., Oates T., Meredith N., and Cochran D.L. Resonance frequency measurement of implant stability in vivo on im-

plants with a sandblasted and acid-etched surface. *Int J Oral Maxillofac Implants*, 18:641–651, 2003.

[98] Pilliar R.M. The effect of partial coating with hydroxyapatite on bone remodelling in relation to porous coated titanium alloy dental implants in the dog. *J Dent Res*, 70:1338–1345, 1991a.

[99] Pilliar R.M., Deporter D.A., Watson P.A., Pharoah M., Chipman M., Valiquette N., Carter S., and Degroot K. Quantitative evaluation of the effect of movement at a porous coated implant-bone interface. *Davies,E. J., Ed. The BoneBiomaterial Interface. Toronto: University of Toronto Press*, pages 380–387, 1991b.

[100] Pilliar R.M., Deporter D.A., Watson P.A., and Valiquette N. Dental implant design-effect on bone remodelling. *Journal of Biomedical Materials Research*, 25:467–493, 1991c.

[101] Truhlar R.S., Lauciello F., Morris H.F., and Ochi S. The influence of bone quality on periotest values of endosseous dental implants at stage ii surgery. *J Oral Maxillofac Surg*, 55:55–61, 1997.

[102] Truhlar R.S, Morris H.F, and Ochi S. Stability of the bone-implant complex. results of longitudinal testing to 60 months with the periotest device on endosseous dental implants. *Ann Periodontol*, 5:42–55, 2000.

[103] Legeros R.Z., Orly I., Gregoire M., and Daculsi G. Substrate surface dissolution and interfacial biological mineralization. *Davies JE, ed. The bone material interface . University of Toronto*, pages 76–88, 1991.

[104] Bhalla S. and Soh C.K. Structural health monitoring by piezo-impedance transducers. i: Modeling. *Journal of Aerospace Engineering*, 17:154–165, 2004.

[105] Bhalla S. and Bajaj S. Bone characterization using piezotransducers as biomedical sensors. *Strain*, 44:475–478, 2008.

[106] Vercaigne S., Wolke J.G., Naert I., and Jansen J.A. The effect of titanium plasma-sprayed implants on trabecular bone healing in the goat. *Biomaterials*, 19:1093–1099, 1998.

[107] Jacobsson S.A., Djerf K., Ivarsson I., and Wahlström O. Effect of diclofenac on fixation of hydroxyapatite-coated implants. an experimental study. *J Bone Joint Surg Br*, 76:831–833, 1994.

[108] Hoshaw S.J., Watson J.T., Schaffler M.B., and Fyhrie D.P. Microdamage at bone-implant interfaces affects bone remodeling activity. *In: Trans 41st Orthop Res Soc, Feb. 13-16 Orlando, FL*, page 188, 1998.

[109] Wheeler S.L. Eight-year clinical retrospective study of titanium plasma-sprayed and hydroxyapatite coated cylinder implants. *Int J Oral Maxillofac. Implants*, 11:340–350, 1996.

[110] Shin S.W., Qureshi A.R., Lee J-Y, and Yun C.B. Piezoelectric sensor based nondestructive active monitoring of strength gain in concrete. *Smart Materials and Structures*, 17:055002, 2008.

[111] Brosh T., Persovski Z., and Binderman I. Mechanical properties of bone-implant interface: an in vitro comparison of the parameters at placement and at 3 months. *Int J Oral Maxillofac Implants*, 10:729–735, 1995.

[112] Jemt T. and Lekholm U. Implant treatment in edentulous maxilla: a five-year follow-up report on patients with different degrees of jaw resorption. *Int J Oral Maxillofac Implants*, 10:303–311, 1993.

[113] Zdeblick T.A., Kunz D.N., Cooke M.E., and McCabe R. Pedicle screw pullout strength. correlation with insertional torque. *Spine (Phila Pa 1976)*, 18:1673–1676, 1993.

[114] Lekholm U. and Zarb G.A. Patient selection and preparation. tissue integrated prostheses: osseointegration in clinical dentistry. *Quintessence Publishing Company*, pages 199–209, 1985.

[115] Giurgiutiu V. and Zagrai A. Embedded active sensors for in-situ structural health monitoring of thin-wall structures. *J Pressure Vessel Techno*, 124:293–302, 2002.

[116] Giurgiutiu V. and Rogers C.A. Recent advancements in the electro-mechanical (e/m) impedance method for structural health monitoring and nde. *SPIE Proceedings of Smart Structures and Materials Conf., San Diego CA*, 3329:536–547, 1998.

[117] Giurgiutiu V., Friedman H., Bender J., Borg T., Yost M., Newcomb W., Black A., Bost J., and Stewart C.

[118] Schulte W. and Lukas D. The periotest method. *Int Dent J*, 42:433–440, 1992.

[119] Schulte W. and Lukas D. Periotest to monitor osseointegration and to check the occlusion in oral implantology. *J Oral Implantol*, 19:23–32, 1993.

[120] Schulte W., d'Hoedt B., Lukas D., Muhlbradt L., Scholz F., Bretschi J., Frey D., Gudat H., Konig M., and Markl M. [periotest–a new measurement process for periodontal function]. *Zahnarztl Mitt*, 73:1229–30, 1233–6, 1239–40, 1983.

[121] Roberts W.E., Simmons K.E., Garetto L.P., and De Castro R.A. Bone physiology and metabolism in dental implantology: Risk factors forosteoporosis and other metabolic bone diseases. *Implant Dent*, 1:11–21, 1992.

[122] Roberts W.E, Smith R.K, and Smith R.S Ziberman Y, Mozsary P.G. Osseous adaptation to continuos loading of rigid endosseous implants. *Am J Orthod*, 86:95–111, 1984.

[123] Ralph W.J. The effects of dental treatment on biting force. *J Prosth Dent*, 41:41–143, 1979.

[124] Isa Z.M. and Hobkirk I.A. Dental implants: biomaterial, biomechanical and biological considerations. *Annual Dent Univ Malaya*, 7:27–35, 2000.